Supplementary Materials for

Development of the annelid axochord: Insights into notochord evolution

Antonella Lauri, Thibaut Brunet, Mette Handberg-Thorsager, Antje H. L. Fischer, Oleg Simakov, Patrick R. H. Steinmetz, Raju Tomer, Philipp J. Keller, Detlev Arendt*

*Corresponding author. E-mail: detlev.arendt@embl.de

Published 12 September 2014, *Science* **345**, 1365 (2014)
DOI: 10.1126/science.1253396

This PDF file includes:

Other Supplementary Material for this manuscript includes the following:
available at www.sciencemag.org/content/345/6202/1365/suppl/DC1

Supplementary Materials:

Material and Methods:

Immunostainings

We developed a protocol for *Platynereis* immunostainings using the Zamboni fixative (*37*). Embryos were fixed either 40 (3 dpf embryos) or 50 minutes (5 days) in cold (4°C) Zamboni fixative (for 20mL: 14.2mL Na_2HPO_4 0.2M, 4 mL NaH_2PO_4 0.2M, 1.3% picric acid, 2.5% paraformaldehyde) at room temperature, washed 5 times in PBS and digested for 1 minute with 100 µg/mL Proteinase K (Merck). Embryos were then washed twice with glycine (2 mg/mL) in PBS, postfixed in Zamboni fixative for 20 minutes at room temperature (25°C), washed 5 times 15 minutes in PBS 0.1% Triton (PBST), blocked 1 hour at room temperature in PBST 5% sheep serum or Roche Blocking Reagent, incubated overnight at 4°C in the primary antibody, washed 5 times in PBST, blocked 1 hour at room temperature and incubated overnight at 4°C in the secondary antibody. Embryos were washed 5 times 15 minutes in PBST and gradually transferred into 80% glycerol DABCO 20% PBS for mounting and imaging. Primary antibodies were: rabbit anti-β-catenin (*38*) (gift of Pierre McCrea, University of Texas), rabbit anti-β-tubulin (gift of Renate Renkawitz-Pohl, Marburg University), and mouse anti-acetylated tubulin (Sigma T9028 1:250). Secondary antibodies were: Dylight 488 anti-rabbit Jackson Laboratories, 1:500 and Dylight 549 anti-mouse (Jackson Laboratories, 1:500). DAPI (1:1000), FM 4-64FX (Invitrogen, 2 µg/mL) and rhodamin-phalloidin (Molecular Probes, 1:500) were used in some stainings in combination with secondary antibodies. Quantification of the fluorescent β-catenin

staining was performed with ImageJ, with DAPI as a counterstain to define the position of the nuclei.

Cloning of *Platynereis* genes

The following primers were used for cloning *Platynereis* genes using a mixed stages *Platynereis* cDNA library (obtained from 1, 2, 3, 5, 6, 10, and 14-days old larvae) and either the HotStart Taq Polymerase from Qiagen or the Phusion polymerase from New England BioLabs (for GC-rich primers).

Gene name	Forward primer	Reverse primer
ColA2	GCTCGAGACAACCCTGCTCGCA	TCAACTGAAACACACAGGACCGAT
FoxD	ACAGAGACTGTGTCATTTCCGTCAC	CTGGGAGGTTTAGAGTCAGAATTGC
Mox	ATGGCCACGCAGAATGGGGGATTGG	TCCTTTGCCATCTGGGCCCCCT
Lamα4	ATGTCAGATGACAGTGGAGGAGC	ATAGAGTGGGTCGTTAGTGTCTG
ColA1	GTGTACCTGGTCTCCAGGGTATGAA	CTGCGCTTGATATCACAGTGAACTT

Twist was cloned by RACE-PCR, using the following forward and reverse RACE (FW1 and R1) and nested (FW2 and R2) primers:

	FW1	FW2	R1	R2
Twist	TCGTGAACGGCAAA	GAAAGATCATCCCC	GTAACTGCAGGACGG	TGCCACTAAAGAAGC

	GGACGCAATCG	ACCCTCCCATC	GGGAATGAGC	GTCGTCGGTC

The following genes were retrieved from an EST collection: *actin*, *mhc1-4*, *mhc11*, *tropomyosin*. Other genes were published earlier: *netrin* (*4*), *foxA* (*39*), *bra* (*9*), *slit* (*4*), *noggin* (*40*) and *hedgehog* (*41*). Orthology of novel genes was checked by molecular phylogeny (Figure S15).

SiMView light-sheet microscopy imaging

An *in vivo* time-lapse recording of a histone-eGFP labelled *Platynereis* embryo was acquired with SiMView light-sheet microscopy (*6*). The zygote was injected with 185 ng/µl H2B-eGFP mRNA and imaged in 100-second intervals. A movie showing maximum-intensity projections of a 30 µm slice of the embryo with manual labeling and tracking of the axochord cells was produced in Imaris.

Whole-mount in situ hybridizations

In situ hybridizations were performed as described (*42*) with the following modifications: larvae were not relaxed (by transfer into 3.75% $MgCl_2$ seawater) before fixation, as relaxation was found to decrease muscle expression of some genes (*foxA*, *brachyury*, *hedgehog*), consistently with the observation that, in vertebrates, gene expression in myocytes is dynamically controlled by contractions (*43*). Immediately after digestion with proteinase K, embryos were acetylated by 5 minutes incubation in 1% triethanolamine, followed by 5 minutes incubation in 1% triethanolamine 0.2% acetic anhydride and by 5 minutes incubation in 1% triethanolamine 0.4% acetic anhydride. Acetylation was found to decrease unspecific binding of the anti-digoxigenin

antibody.

Laser ablations and photoconversion

For both ablation and photoconversion experiments, larvae were briefly (5 minutes) transferred before mounting into 3.75% $MgCl_2$ filtered natural seawater to inhibit muscle contraction (by competitive inhibition of Ca^{2+} by Mg^{2+}). Larvae were then mounted in 3.75% $MgCl_2$ filtered natural sea water, on slides previously coated with 0.5 mg/mL poly-D-lysine in distilled water (P6407 Sigma Aldrich). Poly-D-lysine coating creates an adhesive surface that prevents movements by ciliary beating. Mounted larvae are thus unable to move using either muscles or cilia and are amenable to confocal imaging. Laser ablations were performed using subnanosecond pulses of a 532 nm laser coupled to an Olympus FluoView 1000 inverted confocal microscope. Animals were either co-injected with mYFP and H2A-mCherry or soaked for 12 hours in 2 μM FM 4-64FX (Invitrogen) for live imaging during ablation. *kikGR* mRNA was synthesized from a kikGR-encoding pCS1+ plasmid construct (gift from Atsushi Miyawaki, Riken Centre, Kobe, Japan) using the SP6 mMachine Ambion kit. kikGR photoconversion was performed with pulses of a 405 nm laser at 3% intensity on a Zeiss LSM780 inverted confocal microscope equipped with a photobleaching module. Only kikGR was sufficiently stable for lineage tracking over several days, in contrast to other photoconvertible proteins (Kaede and mEOS).

Microinjection

An agarose stage with a high wall and low wall separated by a 1 mm-wide groove was prepared out of 2% agarose in filtered natural sea water (FNSW) using a microscopy slide and a custom made mold (similar dimensions as the microscopy slide but with a 0.3 mm x 1 mm step on one side). The mold was placed on top of the slide with the step facing down. Liquid 2% agarose was poured next to the slide so that it flows under the mold and polymerizes into a stage of the required shape. After the agarose solidified, the mold was removed, the stage was cut out and placed in the lid of a small Nunclon Surface petri dish. Small scratches in the low wall of the stage, perpendicular to the groove, were manually prepared with a BD Microlance 3 needle under the injection microscope (Zeiss Axiovert 40C inverted microscope, equipped with a micromanipulator and an Eppendorf Femtojet microinjector). Such scratches were found to facilitate needle removal from the eggs after microinjection. The dish was filled with FNSW. 55 min after fertilization the jelly envelope was removed from the zygotes by rinsing them through a net with natural seawater. Then the zygotes were digested for 30 sec with Proteinase K (46 µg/ml) and washed with natural seawater. Digested zygotes were placed in the groove on the agarose stage. The needles used for *Platynereis* are pooled from glass capillaries (borosilicate thin wall with filament, 1.0 mm outer diameter, 0.78 mm inner diameter, Harvard apparatus) using a Sutter needle pooler (with the following parameters: heat 515, pull 025, velocity 120, time 120). During injection, the prepared scratches in the low wall of the agarose stage were used to pull the needle back out of the zygotes. Once the zygotes started cleaving, they were collected into Thermo Scientific 6-well plates (<100 larvae per well in 5 mL FNSW), wrapped into aluminium foil to prevent photobleaching of fluorescent constructs and kept at 18°C.

Transmission electron microscopy

Samples were cryofixed using high pressure freezer HPM-010 at EMBL EM core facility. The freeze substitution was done with 0.2% uranyl acetate, 0.5% osmium, 0.25% glutaraldehyde, 3% water in dehydrated acetone. The following program was used:

Reagent	Time	Temperature
FS solution	24h or longer	-90ºC
FS solution	12h	-90 ºC -> -30 ºC (5ºC/h)
FS solution	3h	-30 ºC
Acetone 100%	3 x 10 min	-30 ºC
Epon:Acetone 1:2	1h	-30 ºC
Epon:Acetone 1:1	1h	-30 ºC
Epon:Acetone 1:2	2h	On ice
Epon pure	1h	On ice
Epon pure	Overnight	Room temperature
Epon pure	1h	Room temperature
polymerisation	48h	60 ºC

The samples were then embedded in moulds, or between Aklar sheets and left in a 60 °C incubator for at least 48 h. Serial sectioning was done with Ultracut (Leica) microtome, producing 70 nm sections. After contrasting with uranyl acetate the sections were imaged on Biotwin CM120 electron microscope.

Vibrotome sections of Platynereis adults

Cross-sections of adult *Platynereis* for Scanning Electron Microscopy observation were produced with a vibrotome. The adults were fixed in Zamboni fixative with 2% of PFA, overnight at 4°C, and then washed 5x5 minutes with PBS. The animals were then embedded in 3% low melting agarose in PBS using a 24 well plate. When the gel was polymerized a squared block of agarose containing the specimens was cut out and glued on the vibrotome holder. The vibrotome chamber was filled with cold PBS. The parameters used for the sections were: 300 μm

(size), 1.40 mm (amplitude), 50mm/s at (speed) to cut the excess of agarose and then 26mm/s to cut samples.

Scanning electron microscopy

Animals were fixed in Zamboni fixative (see Immunostainings section), dehydrated with a series of washes from 20% to 100% acetone and critical point dried in a Leica CPD300 in the Core Facility of Electron Microscopy (Bioquant, University of Heidelberg). The samples were manually put on a SEM holder and the skin was manually removed using tweezers. The specimens were contrasted with gold (10 nm) with a Leica EM MED020 and imaged with a EM LEO1530 using the SE2 detector.

Azakenpaullone treatments

Treated *Platynereis* larvae and the corresponding controls were raised at 18°C in 6 well-plates (Thermo Scientific Nunclon), with about 50 larvae per plate in 5 mL FNSW. Azakenpaullone stocks were kept in DMSO at -20°C. Controls were treated with an equivalent quantity of DMSO. Azakenpaullone treatments were performed from 24 hpf to 48 hpf, at either 2 μM or 5 μM in accordance with the concentrations determined to yield specific phenotypes in previously published studies (*44*).

Clustering analysis

Expression data on the vertebrate structures were compiled from the following resources: ZFIN for zebrafish (http://zfin.org/), Mouse Genetics Institute for mouse (http://www.informatics.jax.org/expression.shtml), GEISHA for chicken

(http://geisha.arizona.edu/geisha/), XenBase for xenopus (http://www.xenbase.org/common/), ANISEED for *Ciona intestinalis* (http://www.aniseed.cnrs.fr/) and gathered from the literature for amphioxus. Clustering analysis of the molecular profiles was performed using MrBayes version 3.2.1 and was run for 1,000,000 generations (until average deviation of split frequencies < 1%) and with constraint of monophyly of Chordates (for floor plate and hypochord), monophyly of Olfactores (for notochord and floor plate) and monophyly of Vertebrates (for notochord, floor plate and hypochord).

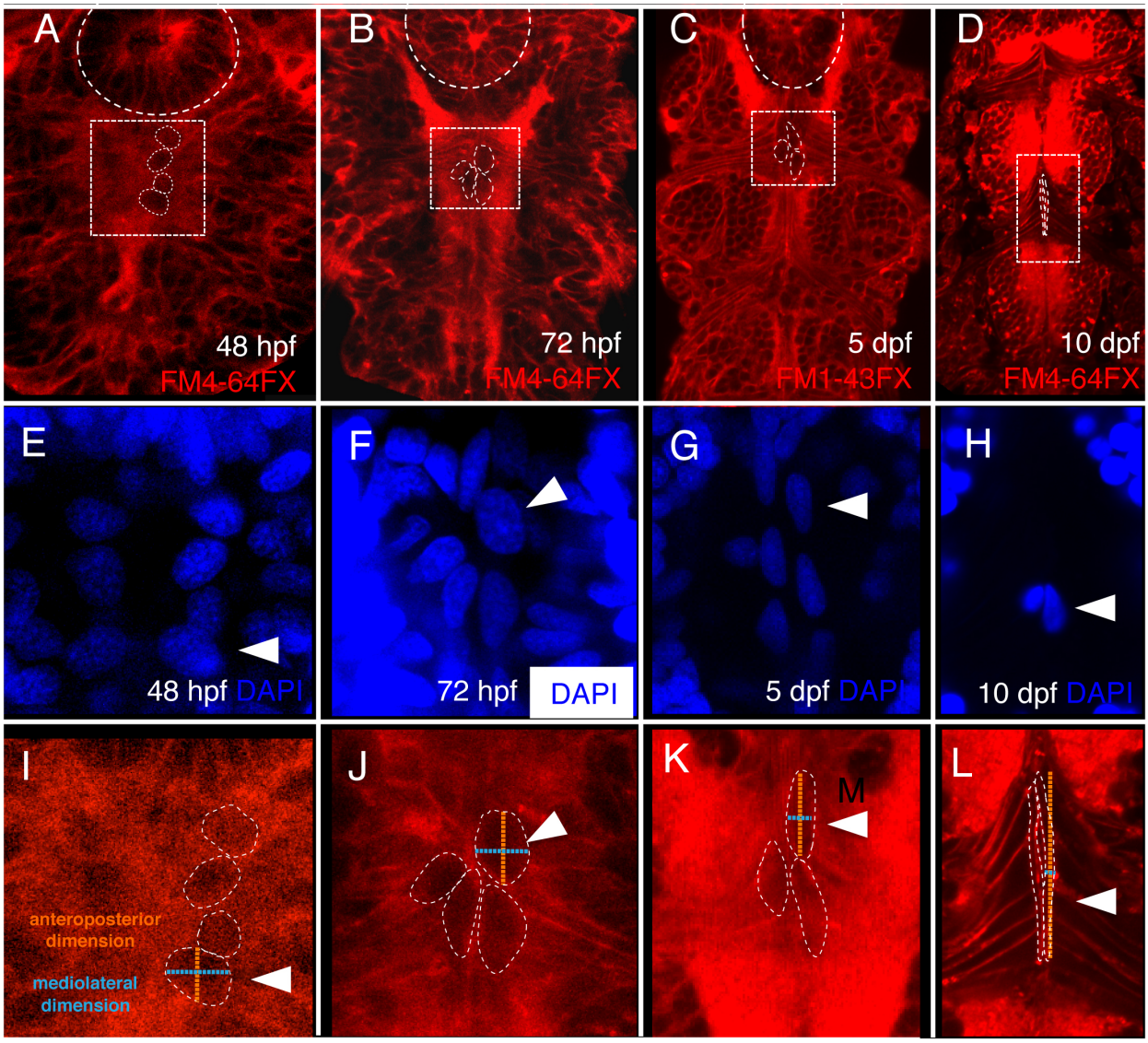
A
48 hpf
FM4-64FX
B
72 hpf
FM4-64FX
C
5 dpf
FM1-43FX
D
10 dpf
FM4-64FX
E
48 hpf DAPI
F
72 hpf
DAPI
G
5 dpf DAPI
H
10 dpf DAPI
I
anteroposterior dimension
mediolateral dimension
J
K
M
L
48 hpf FM4-64FX
72 hpf FM4-64FX
5 dpf FM1-43FX
10 dpf FM4-64FX

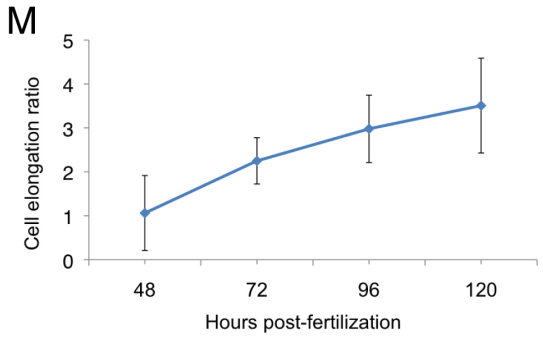
M
Cell elongation ratio
0
1
2
3
4
5
48
72
96
120
Hours post-fertilization

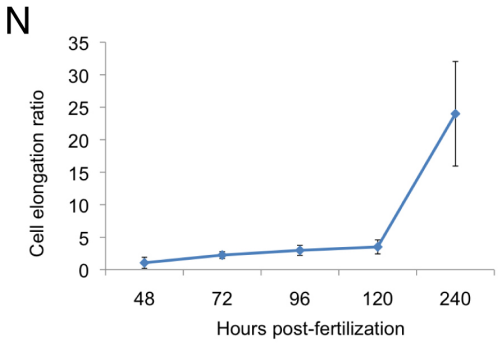
N
Cell elongation ratio
0
5
10
15
20
25
30
35
48
72
96
120
240
Hours post-fertilization

Figure S1. Elongation and narrowing of individual cells contribute to convergence and extension of the axochord. (A-L) z projections of confocal stacks of fixed *Platynereis* larvae stained with FM dyes and DAPI. Membranes are in red and nuclei in blue. Cellular outlines in white stippled lines. Note that the axochord cells are visible as dark shades over the brightly stained neuropil of the nerve cord. (**A-D**) Longitudinal sections at the z-level of the axochord showing whole body of the larvae. White dashed line: foregut. (**E-H**) Close-up on the area in the white dashed square, showing selected axochord nuclei. Arrowhead: nucleus of the axochord cell chosen as example to illustrate the measurements (see I-L). (**I-L**) Same optical sections of the same individuals as E-H, showing membrane signal. Arrowhead: axochord cell chosen as example to illustrate the measurements. Each axochordal cell was measured in its longest dimension along the anteroposterior (orange) and mediolateral (blue) axes. (**M**) Change in cell elongation ratio from 2 dpf to 5 dpf. Cell elongation ratio is defined as (anteroposterior dimension)/(mediolateral dimension). All differences between a time point and the following were significant by Student's *t*-test ($p<0.05$), apart from the 4/5 dpf comparison ($p=0.11$). 5 dpf significantly differs from both 3 dpf ($p=0.0007$) and 10 dpf (see below), which confirms the overall trend. Cells simultaneously become longer and narrower (mediolateral dimension: 12.3±3.4 μm at 2 dpf versus 3.7±1.0 μm at 5 dpf, Student's *t*-test $p=0.0003$; while sectional area does not significantly change: 44.4±16.0 μm^2 versus 39.2±11.1 μm^2, Mann-Whitney's exact test $p=0.56$). (**N**) Same as in M, but showing timecourse until 10 dpf. Between 5 and 10 dpf, the axochord nuclei sink deeply into the tissue, leaving between the commissures only thin and elongated fibres, to which oblique muscles are connected. As the measurements were taken at the level of these more superficial fibres, it results in a very high elongation ratio at 10 dpf, which masks the variation from 2 to 5 dpf. Student's *t*-test $p=0.0007$ for the 5/10 dpf comparison.

	Directed migration	Mediolateral intercalation	Cell elongation	Bipolar to unipolar cell shape change
Frogs	X	√ (*45–48*)	?	√ (*45*) 'Boundary capture' at the axial/paraxial mesoderm boundary
Teleosts	√ 'Dorsal convergence': results first in convergence without extension (shield formation) (*49*) then in convergence-extension. (*7*, *49*)	√ At the dorsal midline after dorsal convergence, results in convergence-extension. (*7*, *49*, *50*)	√ ? In *ntl* mutants, notochord cell elongation drives extension without convergence (radial thinning). Assumed to exist also in wild-type fish. (*50*)	? (*7*)
Ascidians	X (*51*)	√ (*51*, *52*)	√ (*51*, *52*) After mediolateral intercalation. Extension by cell lengthening and narrowing	?
Amphioxus NB: convergence by an amphioxus-specific mechanism of groove formation (*53*)	X? (*53*)	√ ? (*53*) 'Interdigitation' reported by Conklin	√ ? (*53*) 'Cell growth' contributing to notochord elongation reported by Conklin	? (*53*)
Platynereis	√ 'Ventral convergence' similar to fish 'dorsal convergence'	√ At the ventral midline after ventral convergence.	√ After ventral convergence	X? 24 hpf: isotropic *ColA1* mRNA distribution (Fig. 2A) 48 hpf: unipolar *ColA1* mRNA accumulation towards the midline (Fig. 2B). No bipolar configuration observed.

Table S1. Mechanisms underlying axial mesoderm convergence and extension in annelids and chordates

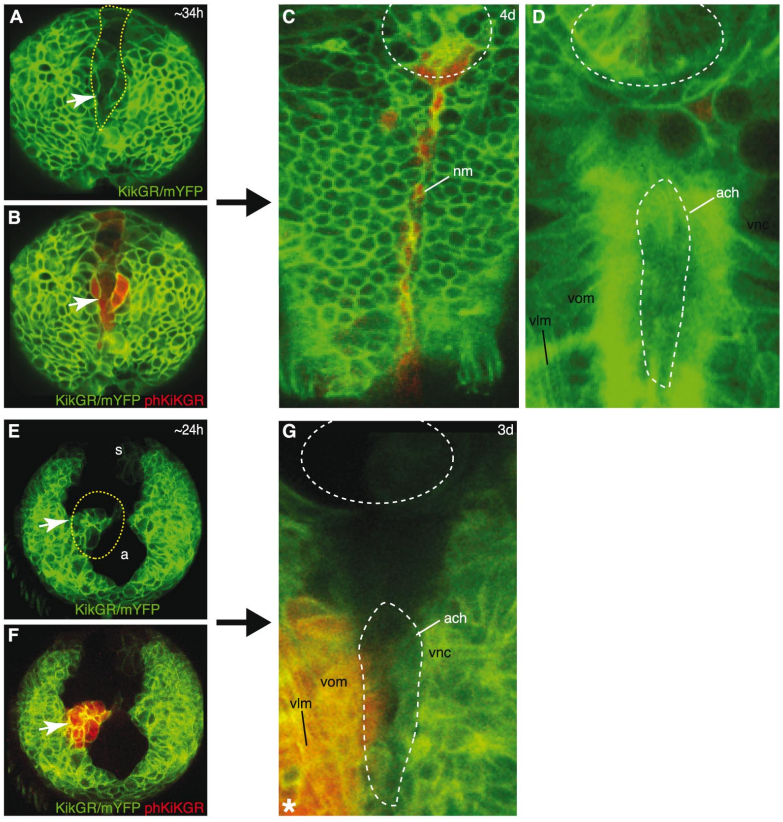

Figure S2. Lineage tracing of the neural midline and of the axochord. All images are z-projections of confocal stacks. (**A**) Ventro-posterior view of a live *Platynereis* larva at around 34 h injected with mRNA for mYFP (membrane, green) and kikGR (cytoplasmic, green). The yellow dashed line outlines the photoconverted area (white arrow). **(B)** Same individual after photoconversion of the superficial midline (photoconverted cells are red, white arrow). **(C)** Ventral view of the same individual after 3 dpf of development showing red labeling in the neuronal midline (*nm*). **(D)** A deeper view showing no labeling in the axochord (*ach*, dashed white line). **(E)** Posterior view (ventral side up) of a live *Platynereis* larva at around 24 h injected as in A. Yellow dashed line outlines the photoconverted area (white arrow). *a*: anus, *s*: stomodeum. **(F)** Same individual after photoconversion of the left mesodermal band (photoconverted cells are red, white arrow). **(G)** Ventral view of the same individual after 3 dpf of development showing red labeling in the axochord (*ach*, dashed white line; inspection of the entire confocal stack confirms identification as axochord cells), the ventral oblique muscles (*vom*) and the ventral longitudinal muscles (*vlm*). During photoconversion of the deep mesodermal bands, a few overlying neuroectodermal cells are unavoidably photoconverted as a side effect (white asterisk). In C, D and G a white dashed circle outlines the stomodeum.

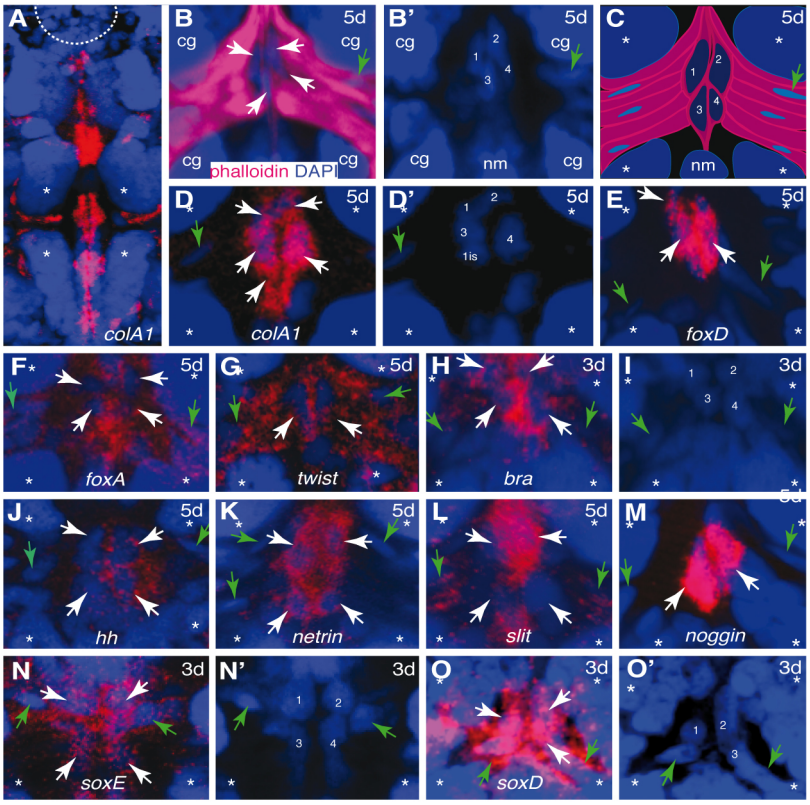

Figure S3. Single WMISH allows identification and expression profiling of individual axochord cells. All panels are z-projections of confocal stacks, ventral view, anterior up. DAPI is in blue and WMISH signal is in red (apart from panels B to D). (**A**) 5 dpf larva stained for *colA1* expression. (**B**) Close-up on the axochord nuclei of the second segment of a 5 dpf larva. Phalloidin signal in red indicates axochord myofibers and shows the muscular nature of axochordal cells. (**B'**) Same as panel B with DAPI signal only. (**C**) Explanatory schematic of panel B. (**D-O'**) Close-up on the axochord nuclei of the second segment of 3 dpf or 5 dpf animals, showing expression of notochordal genes. WMISH signal is red, DAPI is blue. *cg* or asterisks: central ganglia, white arrows: axochord nuclei (1-4: nuclei of the third attachment point, 1is: one intrasegmental nucleus - see Fig. S3), *nm*: neural midline, green arrows: nuclei of the ventral oblique muscles. (**C**) schematic drawing showing the position of the four axochord nuclei of the third attachment point with the myofibers of the axochord and of the ventral oblique muscles (pink). Panels B', D', I, N' and O' are the same views as panel B, D, H, N and O but with DAPI signal only.

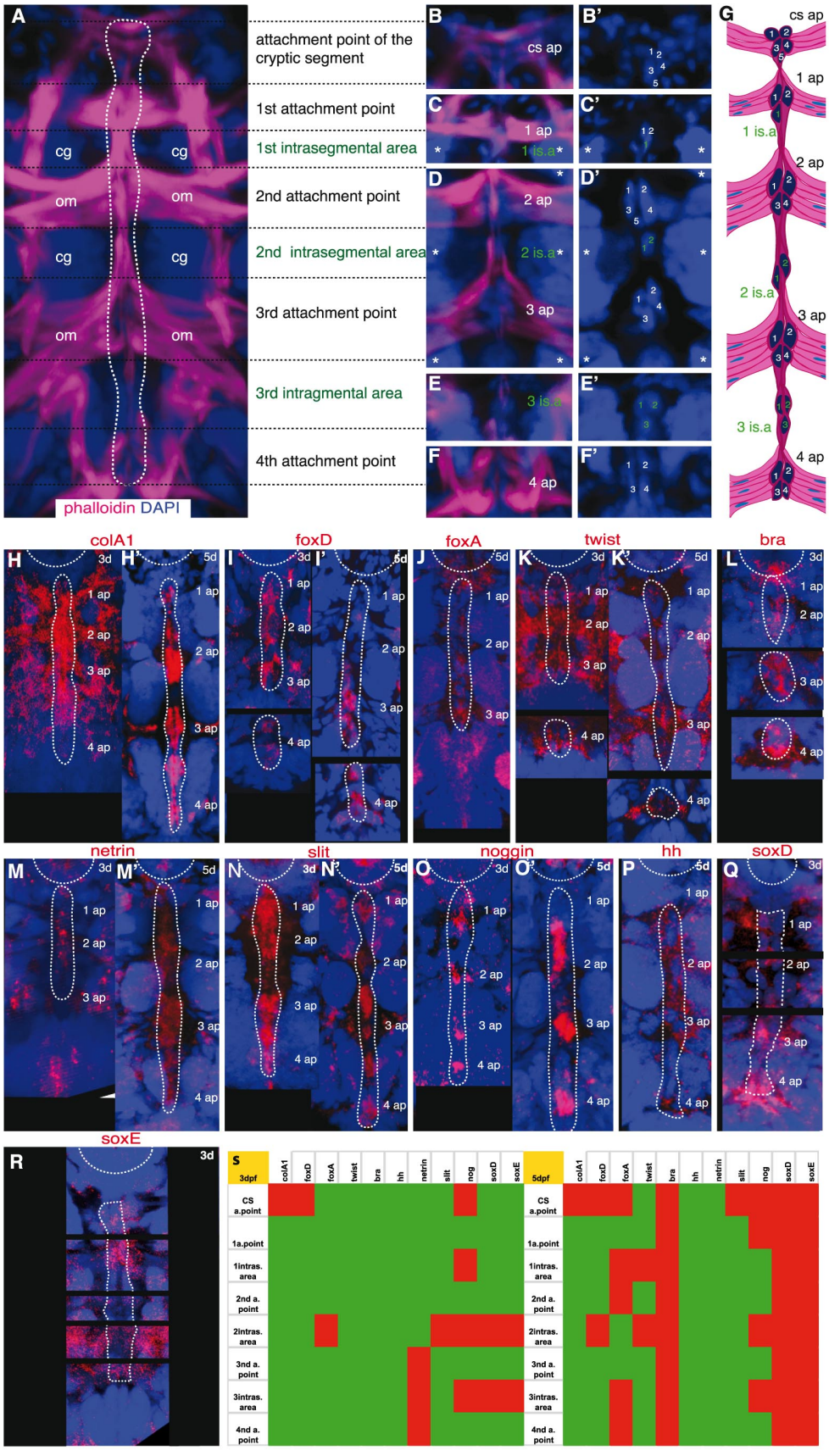
A
attachment point of the cryptic segment
1st attachment point
1st intrasegmental area
2nd attachment point
2nd intrasegmental area
3rd attachment point
3rd intragmental area
4th attachment point
cg
om
phalloidin DAPI
B
B'
C
C'
D
D'
E
E'
F
F'
cs ap
1 ap
1 is.a
2 ap
2 is.a
3 ap
3 is.a
4 ap
G
colA1
foxD
foxA
twist
bra
netrin
slit
noggin
hh
soxD
soxE
3d
5d
R
S
3dpf
5dpf
CS a.point
1a.point
1intras. area
2nd a. point
2intras. area
3nd a. point
3intras. area
4nd a. point

Figure S4: Distinct axochord cell complements, with specific molecular profiles, at different axial levels. All panels apart from G and S are projections of confocal stacks. In A to F', phalloidin is pink, DAPI is blue. **(A)** muscular system of a 5 dpf larva, showing the axochord (white dashed line), the attached oblique muscles (*om*) and the central ganglia (*cg*). Ventral view, anterior is up. Similar to other muscle cells, axochord nuclei are larger than those of the neural cells and elongated in the direction of their myofibers, parallel to the anteroposterior axis. Note that due to the contractility of the axochord (Figure 3B,C), the position and shape of the intrasegmental nuclei can vary between individuals, while the one of attachment points is much more stable. The different subregions of the axochord are labelled on the right next to their axial position. **(B-F)** (respectively **B'-F'**), morphology of the axochordal nuclei with the corresponding myofibers (respectively of the axochordal nuclei only), for each subset of axochordal cells. In C and D, the dashed box outlines the segment shown in Figure 2. **(G)** schematic drawing of axochord and oblique muscles. **(H-R)** (respectively **H'-O'**) z-projections of confocal stacks used for axochord expression profiling of 3 dpf (respectively 5 dpf) larvae. WMISH signal is in red, DAPI is in blue. All panels are ventral views, anterior side up. Dashed white circle is the stomodeum, dashed white line is the axochord. *1ap*: first attachment point. *2ap*: second attachment point. *3ap*: third attachment point. *4ap:* fourth attachment point. The expression signal within the white dashed line represents axochord expression only (as assessed by detailed examination of the nuclei in each of the planes of the z-stack, following the criteria detailed in Fig. 2 and panels A-I in this figure). Note that due do the curved shape of the axochord (depending on its contraction state), axochord nuclei were sometimes located in different planes of the same z-stack and required to combine projections of distinct planes in one given picture to show the full complement of axochord nuclei (in B-F and in I, K, Q and R). **S**, detailed expression profile of each complement of axochord cells at 3 dpf and 5 dpf. *A. point*: attachment point, *CS a. point*: cryptic segment attachment point, *intras. area*: intrasegmental area. Green: gene expression detected via WMISH, red: gene expression not detected.

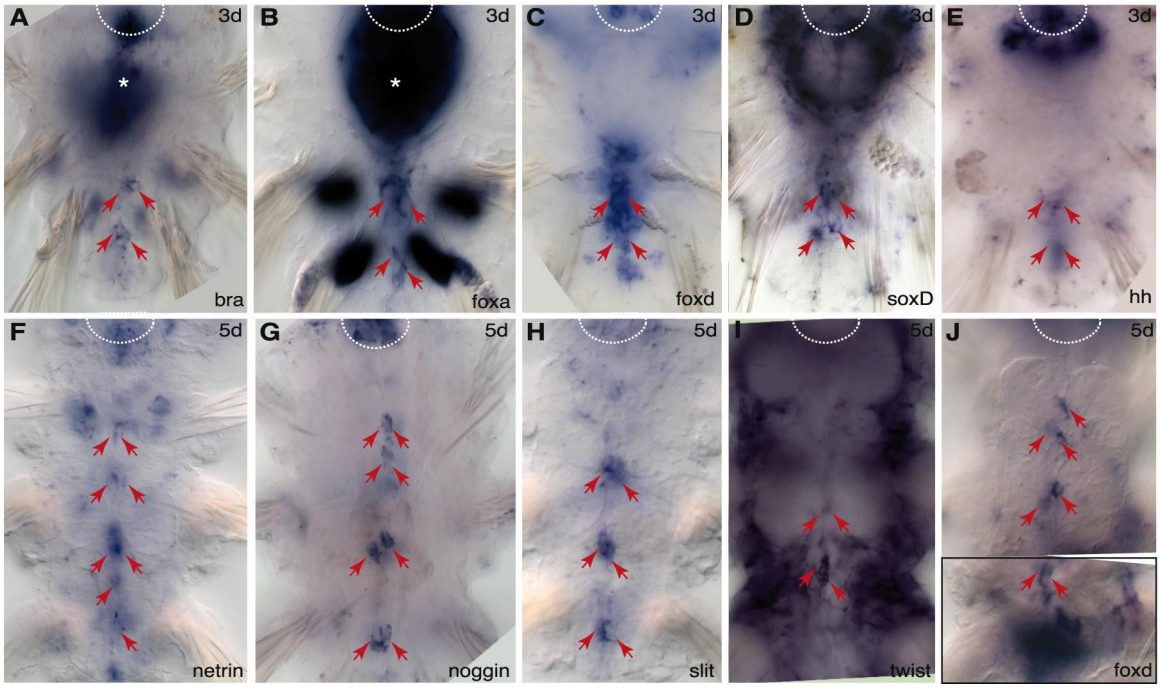

Figure S5. *Platynereis* expression pattern of notochord markers observed in DIC optics. A-J, ventral views of *Platynereis* larvae observed in DIC optics with NBT/BCIP blue precipitate indicating gene expression. In all panels, anterior is up, red arrows indicate expression in midline cells, dashed circle indicates the mouth, asterisk indicates foregut expression.

	Amphioxus	Zebrafish	Xenopus	Chicken	Mouse
Brachyury	**Expression:** Holland et al. (*54*); Terazawa & Satoh (*55*)	**Expression:** Schulte-Merker et al. (*56*) ***4-42 hpf*** **Function:** required for notochord formation (*56*)	**Expression:** Smith et al. (*57*) **Function:** required for notochord formation (*58*)	**Expression:** Kispert et al. (*59*) ***HH4-HH25***	**Expression:** Wilkinson et al. (*60*) ***E7.5- E12.5*** **Function:** required for notochord formation (*60*)
FoxA	**Expression:** Terazawa & Satoh (*55*); Shimeld (*62*)	**Expression:** Odenthal & Nüsslein-Volhard (*62*) ***10.33-16 hpf***	**Expression:** Dirksen & Jamrich (*63*) (*xfkh1*)	**Expression:** GEISHA (*64*) ***HH4-HH17***	**Expression:** Ding et al. (*65*) ***E8-E12.5*** **Function:** required for notochord formation (*66*)
Twist	**Expression:** Yasui et al. (*67*)	**Expression:** Germanguz et al. (*68*) ***6-60 hpf***	**Expression**: Hopwood et al. (*69*) **Function:** required for *Chordin* expression (*70*)	**Expression:** Scaal et al. (*71*) (*cDermo-1*) ***HH7-HH10***	**Expression:** Li et al. (*72*) ***E9***
FoxD	**Expression**: Yu et al. (*73*)	**Expression:** Dutta & Dawid (*74*) (*foxd3*) ***10.33-11.66 hpf***	**Expression:** Sölter et al. (*75*) (*xfd12'*) **Function:** required for notochord formation (*76*)	**Expression:** Khudyakov & Bronner-Fraser (*77*) (*foxd3*) ***HH4-HH10***	**Expression:** Saaki & Hogan (*78*), Tamplin et al. (*79*) (*foxd1*, *foxd2*) ***E8.5-E9***
SoxD	**Expression:** Meulemans & Bronner-Fraser (*80*)	**Expression:** *unreported in the notochord* (*sox13* expression unknown)	**Expression:** *unreported in the notochord* (*sox6* and *sox13* expression unknown)	**Expression:** GEISHA (*64*) (*Sox6*) ***HH7-HH18***	**Expression:** Smits & Lefebvre (*81*) (*Sox5*, *Sox6*) ***E11.5-E15.5*** **Function:** required for notochordal sheath formation (*81*)

SoxE	**Expression:** *unreported in the notochord*	**Expression:** Li et al (*82*) ***– 18 hpf*** (*sox9b*)	**Expression:** Lee & Saint-Jannet (*83*)	**Expression:** McKeown et al. (*84*) ***HH7-HH18***	**Expression:** Ng et al. (*85*) ***E8.5-E12.5*** **Function:** required for notochord maintenance
Slit	**Expression:** *unknown*	**Expression:** Thisse & Thisse (*86*) ***10.33-42 hpf***	**Expression:** Chen et al. (*87*)	**Expression:** Holmes & Niswander (*88*) (*slit2*, *slit3*) ***HH7-HH24***	**Expression:** Holmes et al. (*89*) ***E8.5-E13.5*** **Function:** Midline expression required for commissure formation (*90*)
Netrin	**Expression:** Shimeld (*91*)	**Expression:** Park et al. (*92*) ***11-96 hpf***	**Expression:** *unreported in the notochord*	**Expression:** Kennedy et al. (*93*) ***HH7-HH10*** **Function:** commissure formation (*93*)	**Expression:** *unreported in the notochord*
Hedgehog	**Expression:** Shimeld (*94*)	**Expression:** Krauss et al. (*95*) ***6-60 hpf***	**Expression:** Ekker et al. (*96*)	**Expression:** Marti et al. (*97*) ***HH4-HH30***	**Expression:** Echelard et al. (*98*) ***E7.75-E13.5*** **Function:** neural tube patterning (*99*) and commissure formation (*100*)
Noggin	**Expression:** *unknown*	**Expression:** Fürthauer et al.(*101*) ***10-60 hpf***	**Expression:** Smith & Harland (*102*)	**Expression:** GEISHA(*64*) ***HH4-HH17***	**Expression:** McMahon et al. (*103*) ***E8-E10.5*** **Function:** neural tube patterning (*103*)
ColA	**Expression:** Meulemans & Bronner-Fraser (*80*)	**Expression:** Yan et al. (*104*) ***10-60 hpf***	**Expression:** Su et al. (*105*)	**Expression:** Bendall et al. (*106*),Kosher et al. (*107*) ***HH14-HH44***	**Expression:** Wood et al. (*108*) ***E9-E13.5*** **Function:** inter-vertebral discs formation (*109*)
Coexpressed		**All markers**		**All markers**	**All markers**

		apart from *SoxE*: 11-11.66 hpf		**apart from *ColA*:** HH7-HH10 (*ColA* not investigated in this range)	**apart from *SoxD*:** *E9*

Functional categories:
Notochord specification
Notochord differentiation and structure
Signaling

Table S2. Expression of the notochord markers over five chordate model species.

Coexpression for zebrafish, chicken and mouse was determined according to data from the Zebrafish International Resource Center (http://zfin.org), *Gallus* Expression In Situ Hybridization Analysis (http://geisha.arizona.edu) and Mouse Genetics Informatics (http://www.informatics.jax.org). Not assessed for xenopus and amphioxus due to the absence of centralized databases associating expression sites with systematic staging.

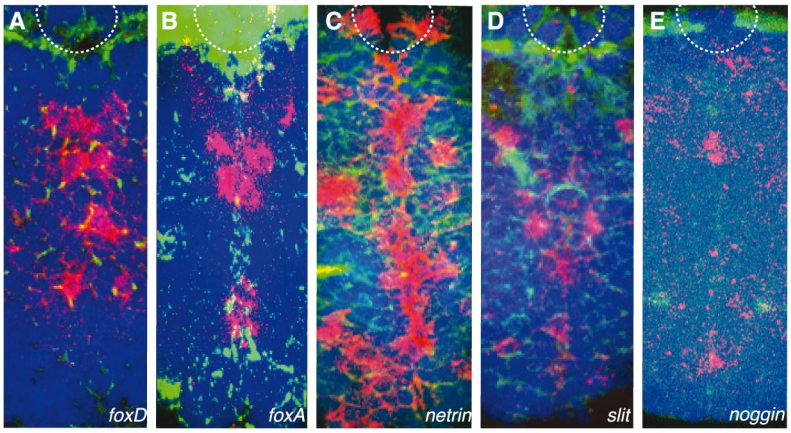

Figure S6. Molecular profile of the neural midline of the *Platynereis* larva. All images are z-projections of confocal stacks, ventral surface views, anterior side up. A-D: 5days, E: 72hpf. WMISH signal is shown in red, tyrosinated tubulin in green and DAPI in blue. **(A)** *FoxD,* **(B)** *FoxA*, **(C)** *Netrin*, **(D)** *Slit,* **(E)** *Noggin.* Dashed white circle indicates the mouth.

A

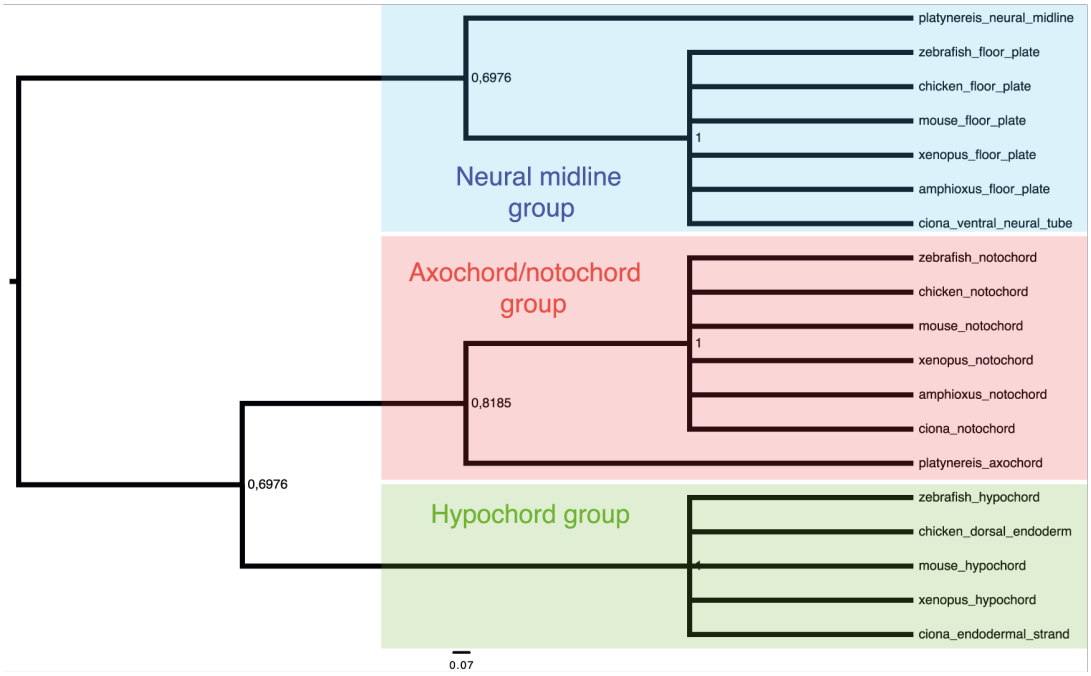
platynereis_neural_midline
zebrafish_floor_plate
chicken_floor_plate
mouse_floor_plate
xenopus_floor_plate
amphioxus_floor_plate
ciona_ventral_neural_tube
0,6976
1
Neural midline group
Axochord/notochord group
zebrafish_notochord
chicken_notochord
mouse_notochord
xenopus_notochord
amphioxus_notochord
ciona_notochord
platynereis_axochord
1
0,8185
0,6976
Hypochord group
zebrafish_hypochord
chicken_dorsal_endoderm
mouse_hypochord
xenopus_hypochord
ciona_endodermal_strand
1
0.07

B

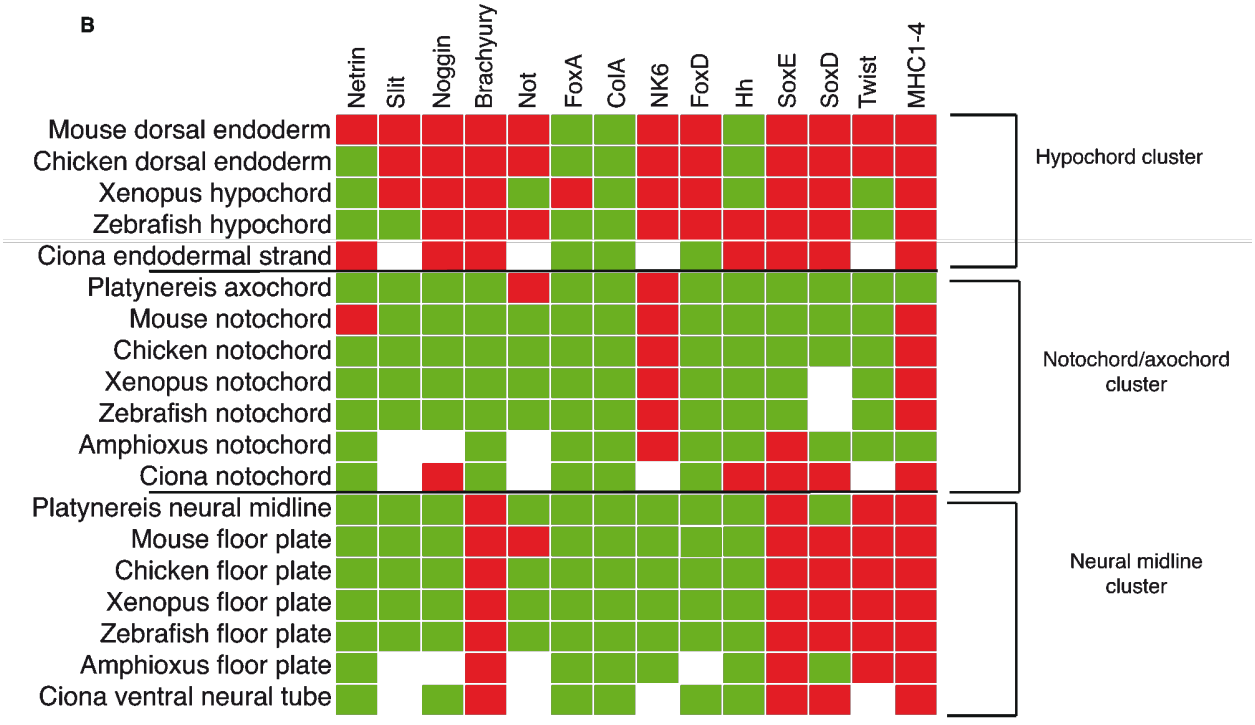
Netrin
Slit
Noggin
Brachyury
Not
FoxA
ColA
NK6
FoxD
Hh
SoxE
SoxD
Twist
MHC1-4
Mouse dorsal endoderm
Chicken dorsal endoderm
Xenopus hypochord
Zebrafish hypochord
Ciona endodermal strand
Platynereis axochord
Mouse notochord
Chicken notochord
Xenopus notochord
Zebrafish notochord
Amphioxus notochord
Ciona notochord
Platynereis neural midline
Mouse floor plate
Chicken floor plate
Xenopus floor plate
Zebrafish floor plate
Amphioxus floor plate
Ciona ventral neural tube
Hypochord cluster
Notochord/axochord cluster
Neural midline cluster

Figure S7. Clustering analysis of molecular profiles of mesodermal midline structures in *Platynereis* and chordates. (A) Clustering analysis of the molecular profiles of mesodermal midline structures in annelids and chordates using MrBayes (see Material and Methods), with neural midlines used collectively as an outgroup, identifies the *Platynereis* neural midline as most closely related to the floor plate with a posterior probability of 0.70 and the axochord as most closely related to the chordate notochord group with a posterior probability of 0.81. **(B)** Molecular profile of the midline structures analyzed. All *Platynereis* expression patterns refer to the same stage (72 hpf).

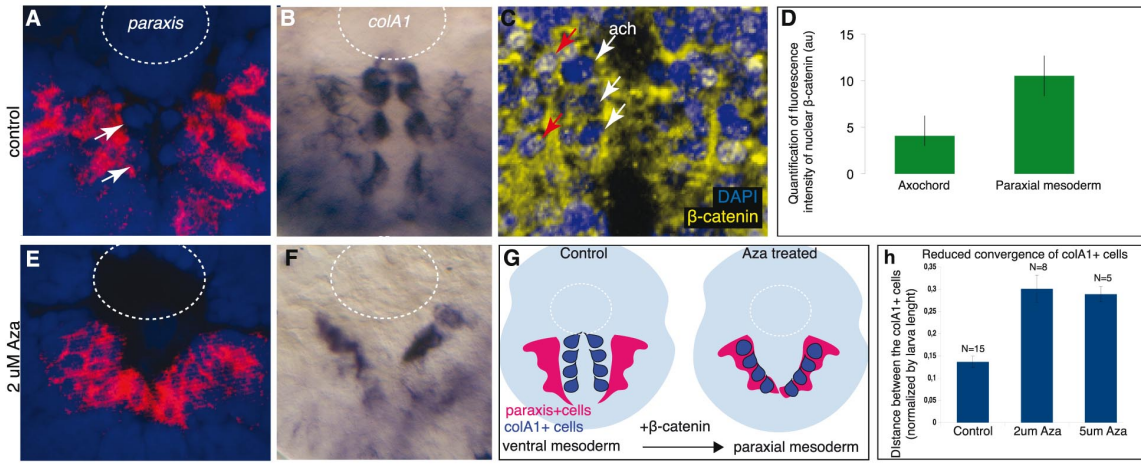

Figure S8. Wnt/β-catenin signaling controls cell sorting and cell identity at the axochord/paraxial mesoderm boundary. (A) Ventral view of *paraxis*+ (red) paraxial mesoderm cells (fated to become the ventral oblique muscles), lateral to the axochord, in a 48 h wild-type *Platynereis* larva. White arrows indicate *paraxis*-negative axochord cells. **(B)** Ventral view of *colA1*+ (WMISH is blue) medial axochord cells in a 48 h wild-type *Platynereis* larva. **(C)** Immunofluorescence, ventral view of β-catenin immunostainings (yellow) of a 48 h larva, revealing a high level of β-catenin nuclear translocation in paraxial mesoderm cells (red arrows), but not in axochord cells (white arrows, *ach*). **(D)** Quantification of the fluorescent β-catenin signal of panel C in the nuclei of the axochord and of paraxial mesoderm (arbitrary units, $p<0.05$ by Mann-Whitney's exact test). **(E)** Ventral view of a 48 h *Platynereis* larva treated with 2 µM azakenpaullone showing *paraxis* expression in the entire mesodermal bands. The lack of mesodermal *paraxis*-negative cells was confirmed by inspection of all confocal z-stacks, demonstrating that the *paraxis* expression pattern includes the non-converged *colA*+ axochord precursors. **(F)** Ventral view of a 48 h *Platynereis* larva treated with 2 µM 1-azakenpaullone (Aza) showing that *ColA1*+ axochord precursors keep a lateral position and stay embedded in the paraxial mesoderm. **(G)** Schematic drawing showing the conversion of axochordal cells towards a paraxial fate and position upon ectopic β-catenin nuclear translocation. (**H**) Quantification of the convergence default of axochord cells in 1-azakenpaullone-treated larvae. Student's *t*-test *p*-value is $3.8*10^{-5}$ (respectively $8.77*10^{-5}$) for controls versus 2 µm (respectively 5 µm) 1-azakenpaullone-treated individuals. A, C and E are z-projections of confocal stacks, DAPI is in blue.

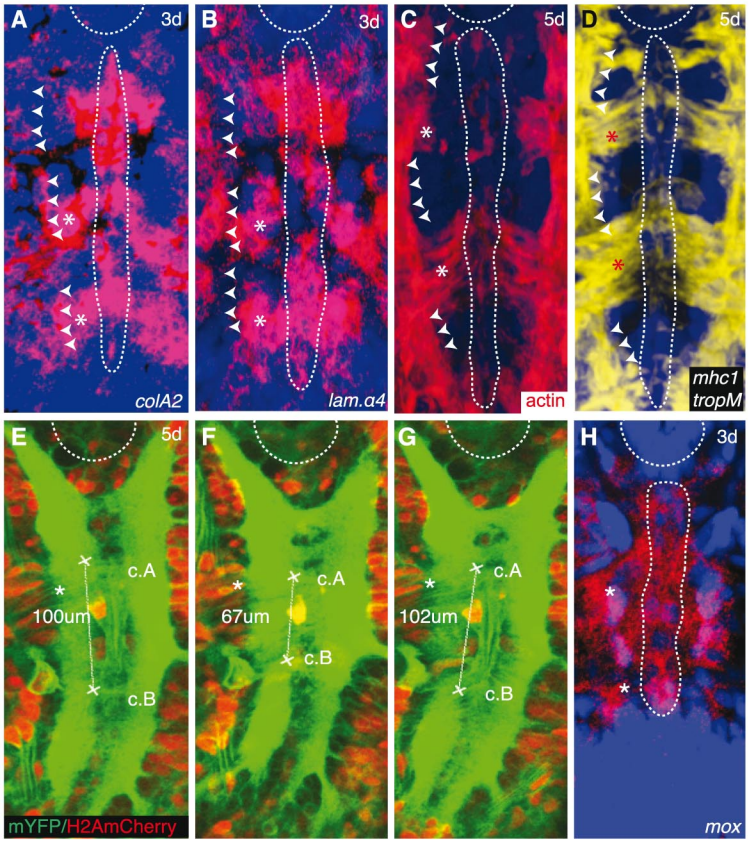

Figure S9. The axochord is a muscle, as shown by live imaging of contractions and expression of muscle markers, and expresses *colA2*, *laminin α4* and *mox*. All images are z-projection of confocal stacks, ventral views. WMISH signal is shown in red in A, B, C, H, in yellow in D, and DAPI is blue. Axochord is indicated with a white dashed line, ventral oblique muscles with an asterisk and ventral longitudinal muscles with white arrowheads. (**A**) *ColA2*. (**B**) *Lam-α4* (laminin α4). (**C**) *Actin*. (**D**) double WMISH of *mhc1-4* and *tropM* (tropomyosin) (co-localization shown in yellow). (**E-G**) Snapshots of a confocal time lapse movie (Supplementary Movie 3) of a juvenile *Platynereis* injected with of H2A-mCherry (red) and mYFP (green). Contraction and relaxation of the axochord can be quantified by measuring the distance (in μm) between commissures A and B (*c. A, c. B*) in consecutive snapshots. (**H**) *Mox* expression in the axochord and the ventral oblique muscles.

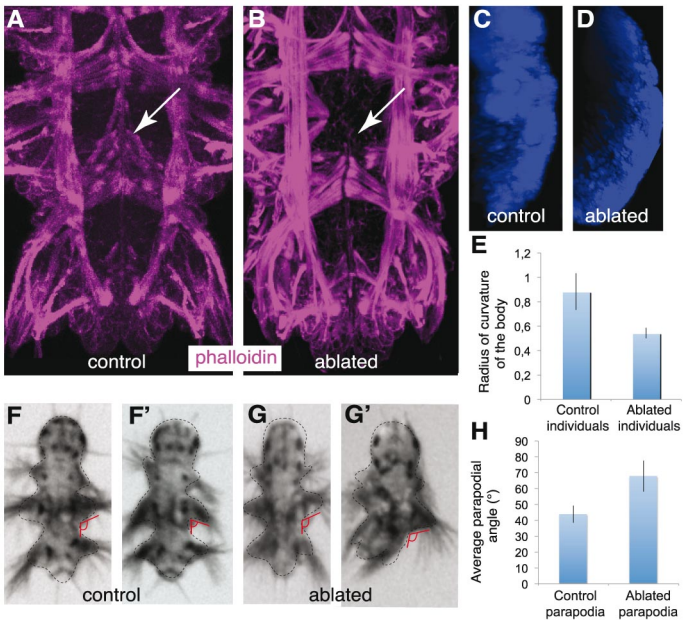

Figure S10. Ablation of axochordal cells disturbs parapodial movements. A-D are immunofluorescence of 5 days larvae. (**A**) Muscles, including the axochord (white arrow) labelled by phalloidin (pink). (**B**) White arrow indicates the missing axochordal cells in the second segment after laser ablation. (**C**) Lateral view of a non-ablated control individual stained with DAPI (blue). (**D**) Lateral view of an ablated individual, ventral side on the left, anterior side up. Note the strong curvature of the ventral side of the body (compare to C). A-D are z-projections of confocal stacks (**E**) Measurements of the radius of curvature of the body in control (n=5) and ablated (n=5) individuals. Student's t-test p-value is 3.1%. (**F-G'**) Dorsal views. Two snapshots of a movie of a wild type animal (F, F') and an animal after axochord ablation (G, G'), showing parapodial movement during crawling behaviour at 5 day. In the ablated animals parapodia remain perpendicular to the body (as shown by the angle in red). Dashed line: body outline. (**H**) Measurements of the angle between the parapodium and the body for ablated parapodia and non-ablated parapodia (internal controls) of the same individuals (n=5). Student's t-test p-value is 1.4%.

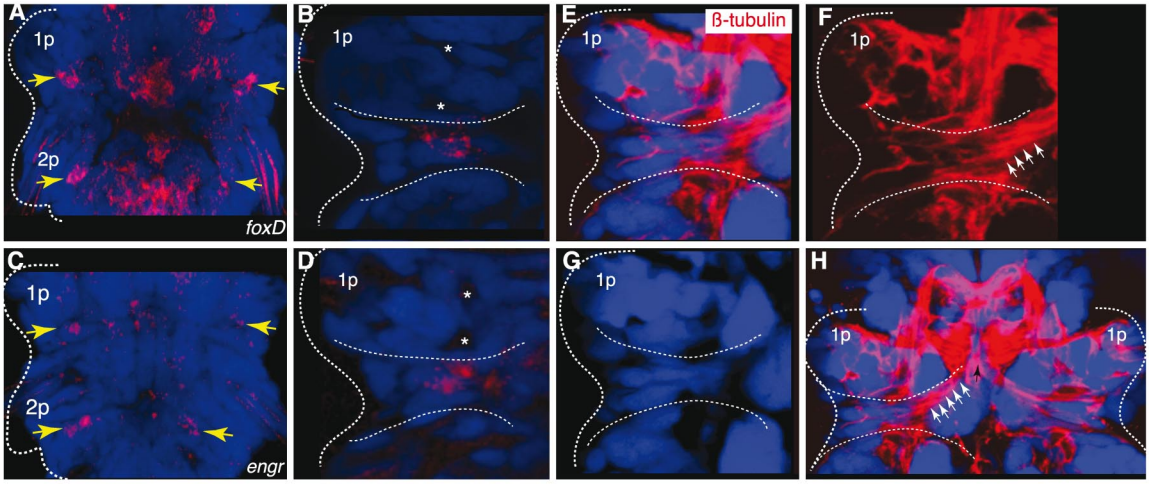

Figure S11. Ventral oblique muscles are uniquely characterized by *engrailed* and *foxD* coexpression. A-D (respectively E-H) are z-projections of confocal stacks of 3 dpf *Platynereis* larvae with DAPI in blue and WMISH (respectively immunostaining) signal in red. All images are ventral views with anterior side up. (**A**) Overview of first two parapodial trunk segments and the corresponding parapodia (1p and 2p) showing *foxD* expression (red) in the posterior ventral oblique muscles (yellow arrows). (**B**) Zoom on the right first parapodium detailing *foxd* expression (red) in the posterior ventral oblique muscles. Dashed lines outline the ventral oblique muscle between the first and second segment as visualized by β-tubulin staining, which specifically stains muscles in *Drosophila* (*78*) and *Platynereis* (compare E-H). Asterisks indicate large cells at the base of chaetal sacs, providing another landmark. (**C**) Overview of the two first trunk segments and the corresponding parapodia (1p and 2p) showing *engrailed* expression (red) in the posterior ventral oblique muscles (yellow arrows). (**D**) Zoom on the right first parapodium detailing *engrailed* expression in the posterior ventral oblique muscles. Dashed lines and asterisks are as in B. (**E**) Ventral view on the right first parapodium showing β–tubulin immunostaining in the posterior ventral oblique muscles, confirming the muscular nature of the nuclei identified (compare with B, D). (**F**) Same view as E, showing β-tubulin staining only. Note that the myofibers of the posterior ventral oblique muscles extend medially (white arrows) to reach their axochordal attachment point (see H). (**G**) Same view as E, showing DAPI staining only for comparison with B, D. (**H**) Ventral view of the same individual as in E-G. Note that the myofibers of the posterior ventral oblique muscles (whose *en*+ *foxd*+ nuclei are located peripherally in between the parapodia) extend medially (white arrows) to reach their axochordal attachment point (black arrow).

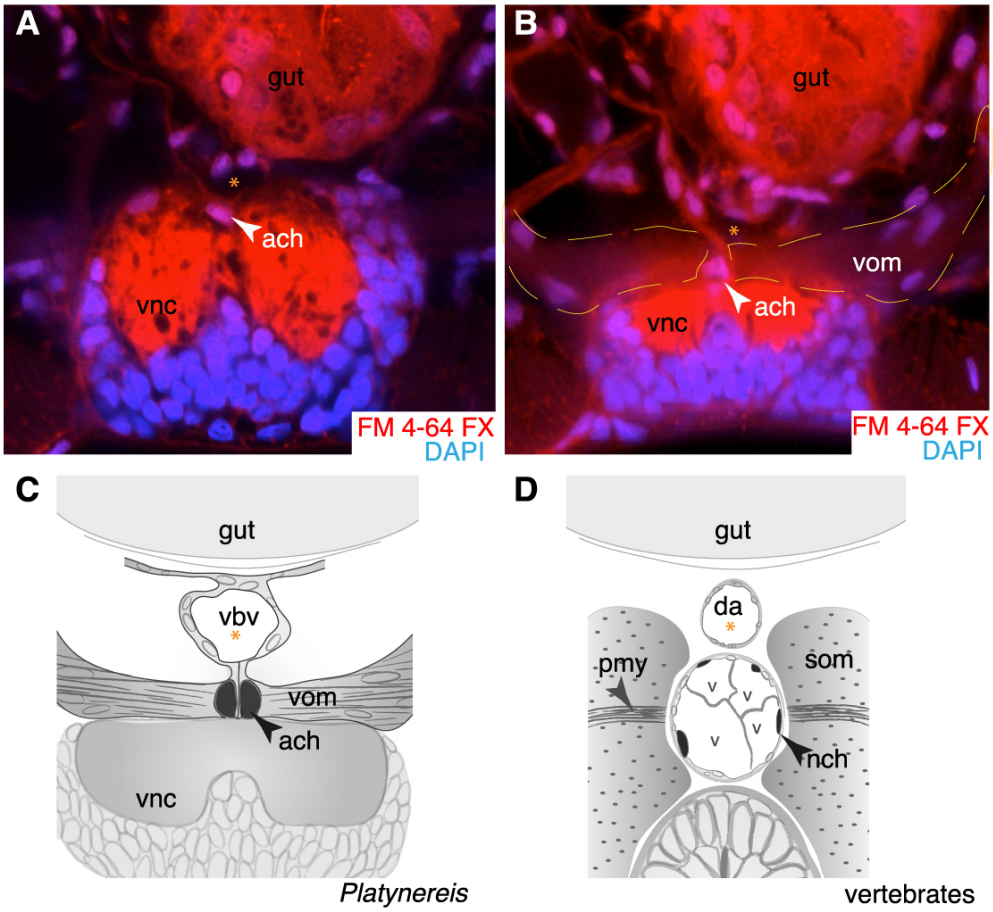

Figure S12. Cross sections of the adult Platynereis trunk. A and B are z-projections of confocal stacks. (**A**) Cross sections of a 12 segments (12 s; about 1 month old) old juvenile labeled with FM 4-64FX (red) and DAPI (blue); ventral is down. The ventral blood vessel (orange asterisk) is first visible at this stage between the axochord (*ach*) and gut. *vnc:* ventral nerve cord. (**B**) Cross section of the same individual as in A at another anteroposterior level, showing the attachment of ventral oblique muscles (*vom*, outlined by yellow dotted lines). (**C,D**) Explanatory schematics showing anatomical position and cellular morphology of the axochord compared to the notochord. Abbreviations in C are as in A and B. In D, orange asterisk indicates the dorsal aorta. *pmy*: pioneer myocytes, *nch*: notochord, *som*: somites, *da*: dorsal aorta, *v*: vacuoles.

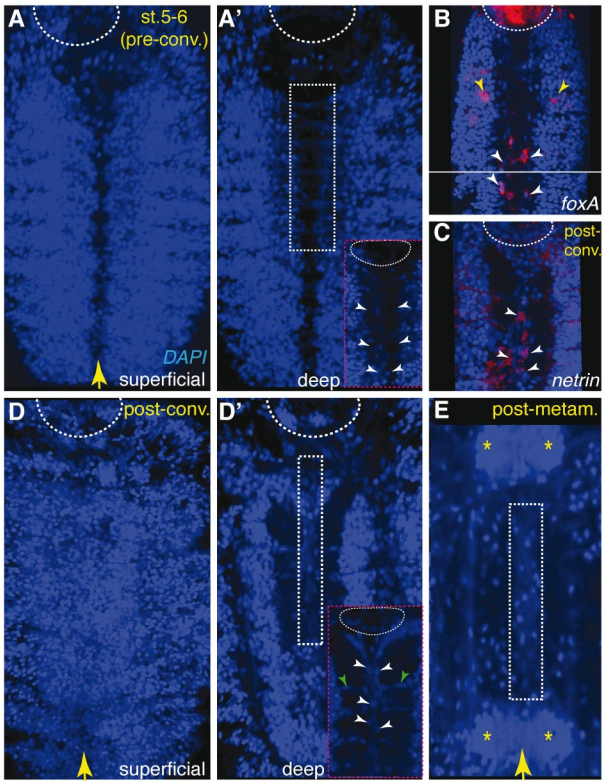

Figure S13. Convergence of the *Capitella* paramedian muscle into an axochord, and *foxA* and *netrin* expression. Z-projections of confocal stacks, ventral view, anterior up. Blue is DAPI and red (B and C) is WMISH signal. Dashed line indicates the stomodeum. (**A**) Superficial view of a stage 5-6 larva showing the open neural midline (yellow arrow). (**A'**) Deep view of the same individual showing the non-converged nuclei of the paramedian muscle. Red square: close-up of the area within the dashed white square, showing paramedian muscle nuclei (white arrowheads). (**B**) *foxA* expression in paramedian muscle cells before convergence (white arrowheads). Note expression in scattered ectodermal cells (yellow arrowheads). (**C**) *netrin* expression in axochord cells after convergence (see below). (**D**) Superficial view of a stage 8-9 larva showing the closed neural midline (yellow arrow). (**D'**) Deep view of the same individual showing the converged axochord nuclei. Red square: close-up of the area within the dashed white square, showing the converged axochord nuclei (white arrowheads). Note the perpendicular orientation of the oblique muscles nuclei (green arrowheads). (**E**) Deep ventral view of a post-metamorphic (post-settlement) *Capitella* larva, showing axochord nuclei within the dashed white square. Yellow asterisks: central ganglia. Yellow line: neural midline.

Phylum	Presence of axial longitudinal muscles
Chordata	**Notochord**, near-universally present, muscular in amphioxus (*111*)
Hemichordata	**Ventromedian muscle**: *Protoglossus* (*112*, *113*) (referred to as *Protobalanus* in the original publication) **Paramedian muscle:** *Saccoglossus*, *Balanoglossus* (*112*), *Cephalodiscus* (*114*) Ventromedian and paramedian muscles share the same quality (longitudinal striated muscles) and the same connections with other organs (as the median edge of the ventral muscle mass, ventral to the blood vessel and dorsal to the ventral nerve cord). The transition between both configurations most likely reflects variable degrees of convergence.
Echinodermata	No candidate ventromedian muscle (*115*)
Chaetognatha	**Ventromedian muscle**: repeated pair of elongated, triangular muscular cells in the ventral midline, connected to the ventral mesentery (*116*, *117*)
Loricifera	No candidate ventromedian muscle (*118*)
Kinorhyncha	**Paramedian muscle** pair of fibers immediately flanking the midline and serving as an attachment point for ventral transverse muscles (*119*)
Priapulida	**Continuous longitudinal muscle layer** (*120*)
Nematoda	**Continuous longitudinal muscle layer** (*120*)
Nematomorpha	**Continuous longitudinal muscle layer** (*120*)
Tardigrada	**Ventromedian longitudinal muscle** in the first segment, bordering ventrally the pharynx in *Macrobiotus* (*122*)
Onychophora	**Ventromedian muscle** (*123*)
Arthropoda	**Ventromedian mesodermal midline glia**: *Drosophila*. Segmentally repeated pairs of cells immediately underlying the ventral nerve chord, secreting an abundant extracellular matrix (including laminin and collagen), required for commissural axon guidance and specifically expressing the homeobox gene *mox/ buttonless* (*124*) (also expressed in the *Platynereis* axochord, see Fig. S9H).
Brachiopoda	**Ventromedian muscle**: *Argyrotheca* larvae (*24*)
Phoronida	**Ventromedian muscle**: median longitudinal fibers bordering the ventral side of the gut of *Phoronis pallida* (*125*)
Ectoprocta	NA (*no unambiguous assignment of dorsal or ventral sides*)
Cycliophora	**Ventromedian muscle** (vacuolated "chordoid organ") (*126–128*)
Entoprocta	NA (*no unambiguous assignment of dorsal or ventral sides*)
Rotifera	**Ventromedian muscle:** *Proales daphnicola* and *Brachionus urceolaris*. Formed by a pair of bilateral myofibers contacting each other in the midline and diverging at their anterior and posterior extremities (*129*, *130*) **Paramedian muscle:** *Dicranophorus* (*131*). Pairs of fibers meeting

	in the midline at their posterior attachment point, and attaching anteriorly at the corona boundary, like the ventromedian muscle in other genera, supporting homology of both structures.
Micrognathozoa	*No data on musculature*
Gnathostomulida	**Ventromedian muscle:** in the stylet, formed a pair of bilateral myofibers contacting each other in the midline and diverging in the anterior part of the animal (*132*)
Gastrotricha	**Ventromedian longitudinal muscle:** *Xenotrichula*. Formed by a pair of bilateral myofibers contacting each other in the midline and diverging at their anterior and posterior extremities (*133*, *134*) **Paramedian muscle:** *Draculiciteria*. Pair of fibers flanking the midline (*135*) Both type of muscles represent the ventral-most pair of longitudinal somatic muscles and extend along the whole antero-posterior axis, with anterior paired attachment behind the mouth and posterior divergent extensions into the adhesive tubes, consistently with them being homologous to each other.
Platyhelmintha	**Continuous longitudinal muscle layer** (*121*)
Nemertea	**Continuous longitudinal muscle layer** in adults (*121*) **Ventromedian muscle** in embryos of *Prosorhochmus americanus* (proboscis retractor muscle) (*136*). Early embryos develop first a simple stereotypic pattern comprising circular muscles, a few pairs of lateral longitudinal muscles and a ventromedian muscle, before elaborating a circumferential longitudinal muscle layer.
Mollusca	**Ventromedian muscle:** in both main aplacaphoran clades: Chaetodermomorpha (*Chaetoderma*) (*137*) and Neomeniomorpha (*Pachymenia* (*138*), *Wirenia*) and in polyplacophorans (*Leptochiton*, *Mopalia*) (*23*)
Annelida	**Ventromedian longitudinal muscle** in virtually every family investigated, in both Sedentaria (Serpulidae (*139*), Spionidae (*19*), Sabellidae (*140*) and Capitellidae (*18*)) and Errantia (Magelonidae (*19*), Dorvilleidae (*141*), Nerilidae (*142*), Chrysopetalidae (*143*), Syllidae (*144*), Sphaerodoridae (*144*) and Nereidae (*145*)) **Paramedian longitudinal muscle**: in young *Capitella* larvae (*18*) (becomes unpaired in later development (Fig. 4a-d)) and *Prionospio* (*19*) **Continuous longitudinal muscle layer** in clitellates (*121*) **No candidate ventromedian muscle** revealed by phalloidin stainings in the sipunculid *Themiste* (*146*) (but in situ hybridization indicates the existence of probably non-muscular deep *foxA*+ midline cells (*147*))

Table S3: Phylogenetic distribution of axial longitudinal muscles in bilaterian phyla

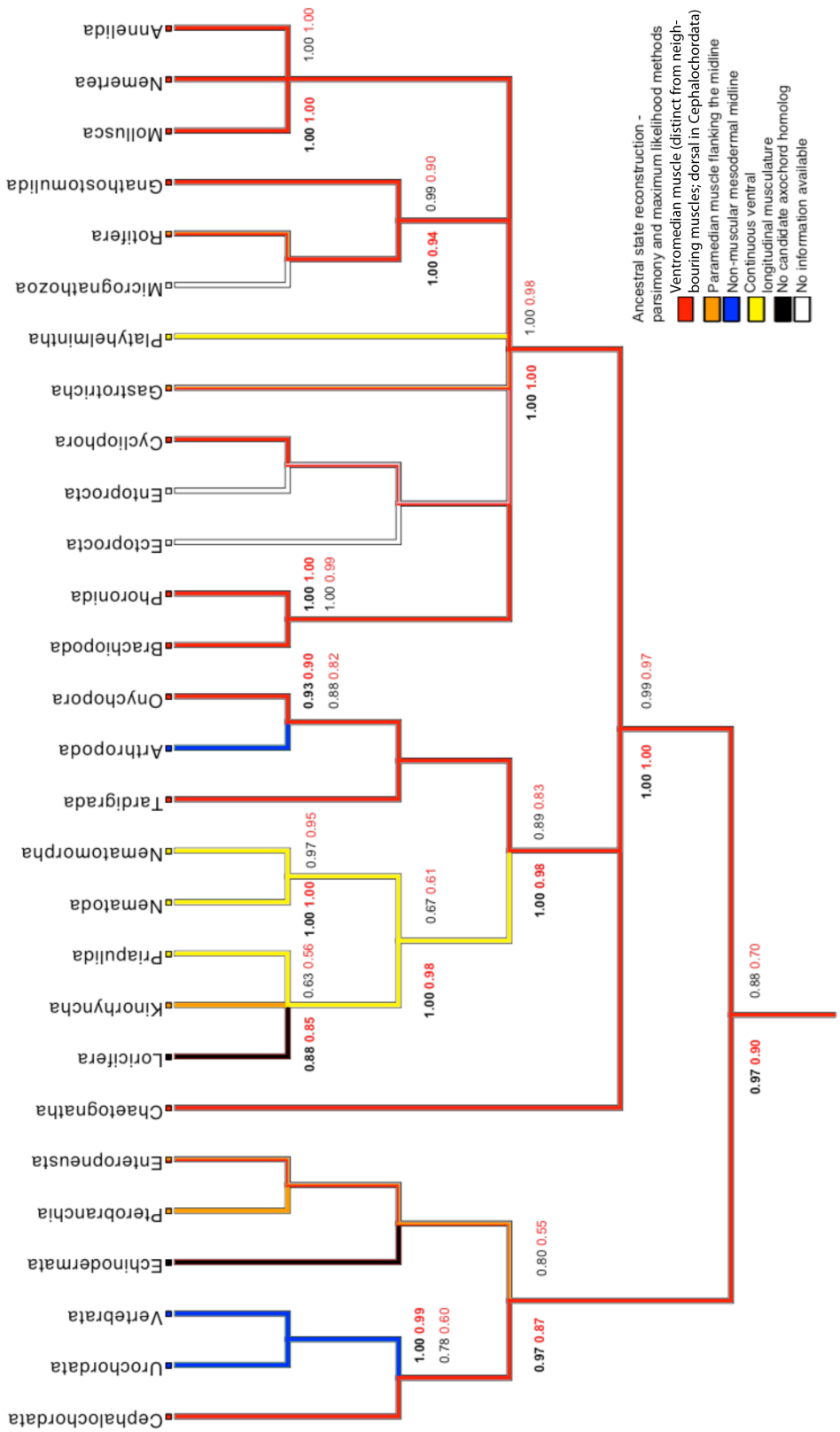
Ancestral state reconstruction - parsimony and maximum likelihood methods
Ventromedian muscle (distinct from neighbouring muscles; dorsal in Cephalochordata)
Paramedian muscle flanking the midline
Non-muscular mesodermal midline
Continuous ventral longitudinal musculature
No candidate axochord homolog
No information available
Cephalochordata
Urochordata
Vertebrata
Echinodermata
Pterobranchia
Enteropneusta
Chaetognatha
Loricifera
Kinorhyncha
Priapulida
Nematoda
Nematomorpha
Tardigrada
Arthropoda
Onychophora
Brachiopoda
Phoronida
Ectoprocta
Entoprocta
Cycliophora
Gastrotricha
Platyhelminthes
Micrognathozoa
Rotifera
Gnathostomulida
Mollusca
Nemertea
Annelida

Figure S14. Phylogenetic distribution and ancestral state for ventral musculature in Bilateria. Ventromedian longitudinal muscles were counted as axochord if they span the midline along a significant part of their length, but can diverge into paired fibers at their anterior or posterior ends (as the axochord of the annelid *Pomatoceros* (*148*)). Ancestral state reconstruction was performed with Mesquite 2.75, using parsimony and Maximum Likelihood (ML) methods. Both methods yielded the same ancestral state for all nodes. Proportional Likelihood (PL) indicated in bold black numbers for the general presence of ventromedian myofibers and in regular black numbers for the presence of a distinct ventromedian muscle not embedded in a continuous longitudinal muscle layer. Numbers in red indicate PL under conservative assumptions (with enteropneusts, rotifers and gastrotrichs counted as paramedian). The bilaterian phylogenetic tree is following Nielsen (*149*). The inferred bilaterian ancestral state is robust to alternative tree topologies (Figure S14). All bilaterian phyla, apart from Echinodermata, Loricifera, and the insufficiently studied Micrognathozoa, possess ventromedian mesodermal cells on the neural side (dorsal in chordates and ventral in non-chordates). No character state is proposed for ectoprocts and entoprocts, since assignment of ventral or dorsal sides in these phyla is uncertain. Coloring of branches indicates that axial mesodermal cells have been reported in at least some members of the phylum but not necessarily in all (e.g. some chordates, such as the direct-developing tailless ascidian *Molgula occulta*, have lost the notochord; moreover the axochord can easily be overlooked, as it was until recently in polyplacophoran mollusks (*23*)). By comparison to the annelid situation, paramedian muscles were defined as pairs of ventral muscles flanking the midline. For annelids, the most parsimonious ancestral state is the presence of a distinct axochord, as other character states are present in a minority of scattered species (see Table S3). Three other phyla similarly show mixed character states: Gastrotricha, Rotifera and Enteropneusta (indicated by double colors in the tree; Table S3). In those three phyla, homology of ventromedian and paramedian muscles is supported by the fact they never coexist, by the existence of a continuum of intermediate configurations across species (with varying levels of convergence) and sometimes within species (e.g. in ontogeny as in *Capitella*, or along the antero-posterior axis as in *Pomatoceros*), and by their identical connections to the rest of the musculature (Table S3). Under both configurations, those muscles thus represent reasonable candidate axochord homologs. As the internal phylogeny of these three groups is still poorly known, either configuration could represent the primitive state. Regardless of which

configuration is primitive for these three phyla, presence of a ventromedian longitudinal muscle is the most parsimonious ancestral state for Bilateria.

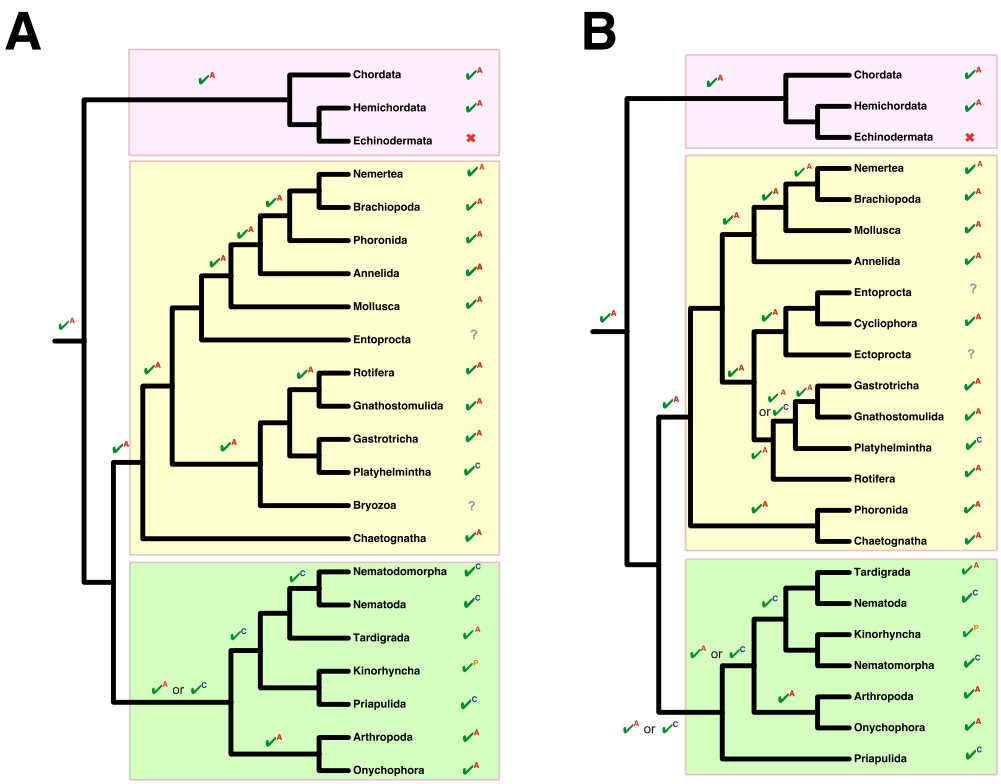

Figure S15. The hypothesis of the ancestrality of a ventromedian muscle is robust to uncertainties about high-level metazoan phylogeny. Green ticks indicate the presence of a candidate axochord homolog, with letters in exponent detailing the character state: A: axochord clearly distinct from the rest of the musculature; C: continuous longitudinal muscle layer; P: paramedian muscle flanking the midline. Red crosses indicate the absence of any candidate axochord homolog. Ancestral character states for each node were inferred using the parsimony method. (**A**) metazoan phylogeny according to Dunn et al. (*150*) (**B**) metazoan phylogeny according to Hejnol et al. (*151*) In both panels, Deuterostomia are pink, Lophotrochozoa are yellow and Ecdysozoa are green. Character states are as in Figure S13, with ventromedian muscle being assumed to be the primitive state for enteropneusts, gastrotrichs and rotifers, which show coexistence with paramedian muscles. Note that assuming paramedian muscles instead to be the primitive state for those phyla would not affect this conclusion.

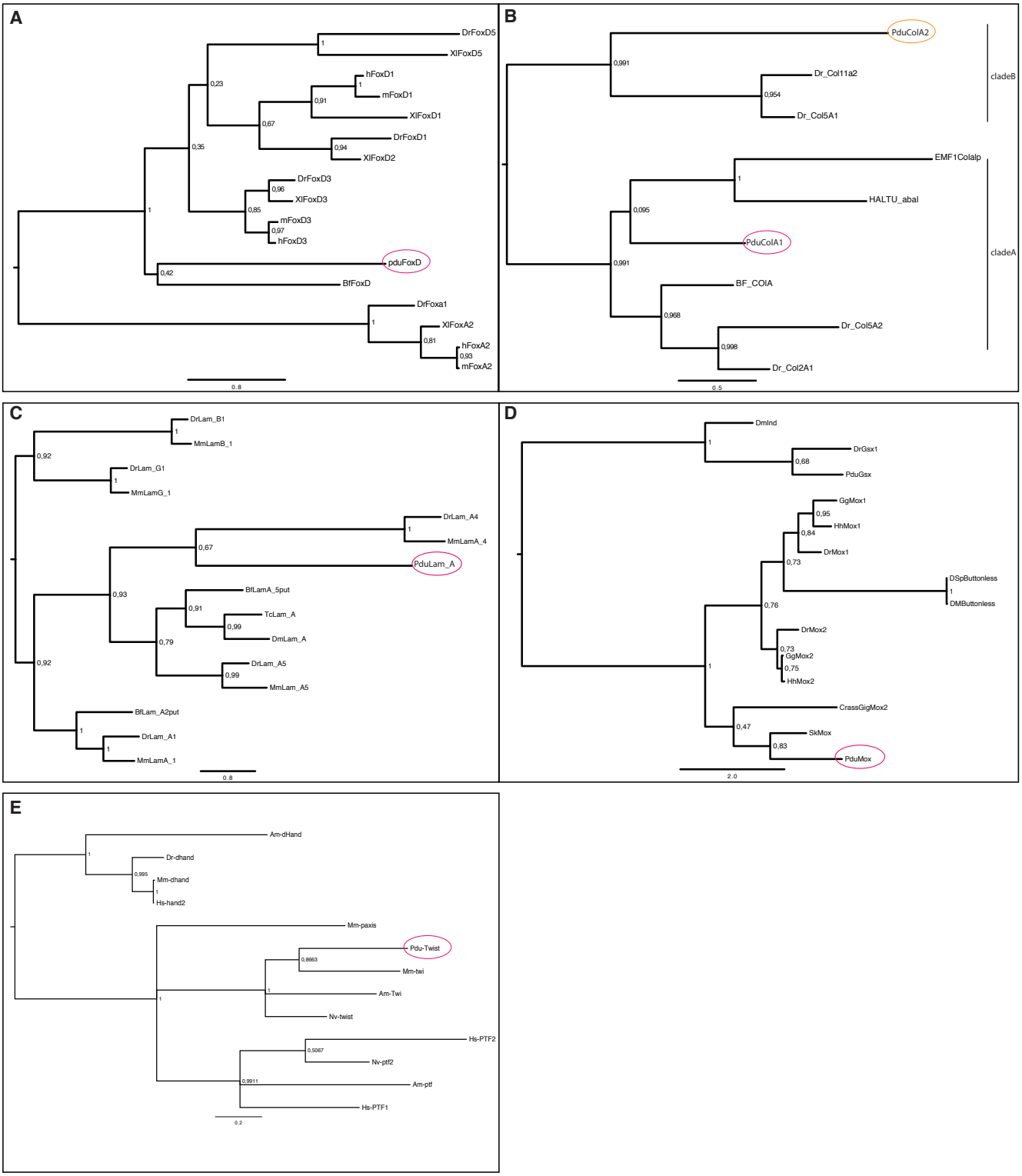
A
DrFoxD5
XlFoxD5
hFoxD1
mFoxD1
XlFoxD1
DrFoxD1
XlFoxD2
DrFoxD3
XlFoxD3
mFoxD3
hFoxD3
pduFoxD
BfFoxD
DrFoxa1
XlFoxA2
hFoxA2
mFoxA2
0.23
0.67
0.35
0.91
0.94
0.96
0.85
0.97
0.42
0.81
0.93
0.8
B
PduColA2
Dr_Col11a2
Dr_Col5A1
EMF1ColaIp
HALTU_abal
PduColA1
BF_COIA
Dr_Col5A2
Dr_Col2A1
cladeB
cladeA
0.991
0.954
0.095
0.968
0.998
0.5
C
DrLam_B1
MmLamB_1
DrLam_G1
MmLamG_1
DrLam_A4
MmLamA_4
PduLam_A
BfLamA_5put
TcLam_A
DmLam_A
DrLam_A5
MmLam_A5
BfLam_A2put
DrLam_A1
MmLamA_1
0.92
0.67
0.93
0.91
0.99
0.79
0.8
D
DmInd
DrGsx1
PduGsx
GgMox1
HhMox1
DrMox1
DSpButtonless
DMButtonless
DrMox2
GgMox2
HhMox2
CrassGigMox2
SkMox
PduMox
0.68
0.95
0.84
0.73
0.76
0.75
0.47
0.83
2.0
E
Am-dHand
Dr-dhand
Mm-dhand
Hs-hand2
Mm-paxis
Pdu-Twist
Mm-twi
Am-Twi
Nv-twist
Hs-PTF2
Nv-ptf2
Am-ptf
Hs-PTF1
0.995
0.8663
0.5067
0.9911
0.2

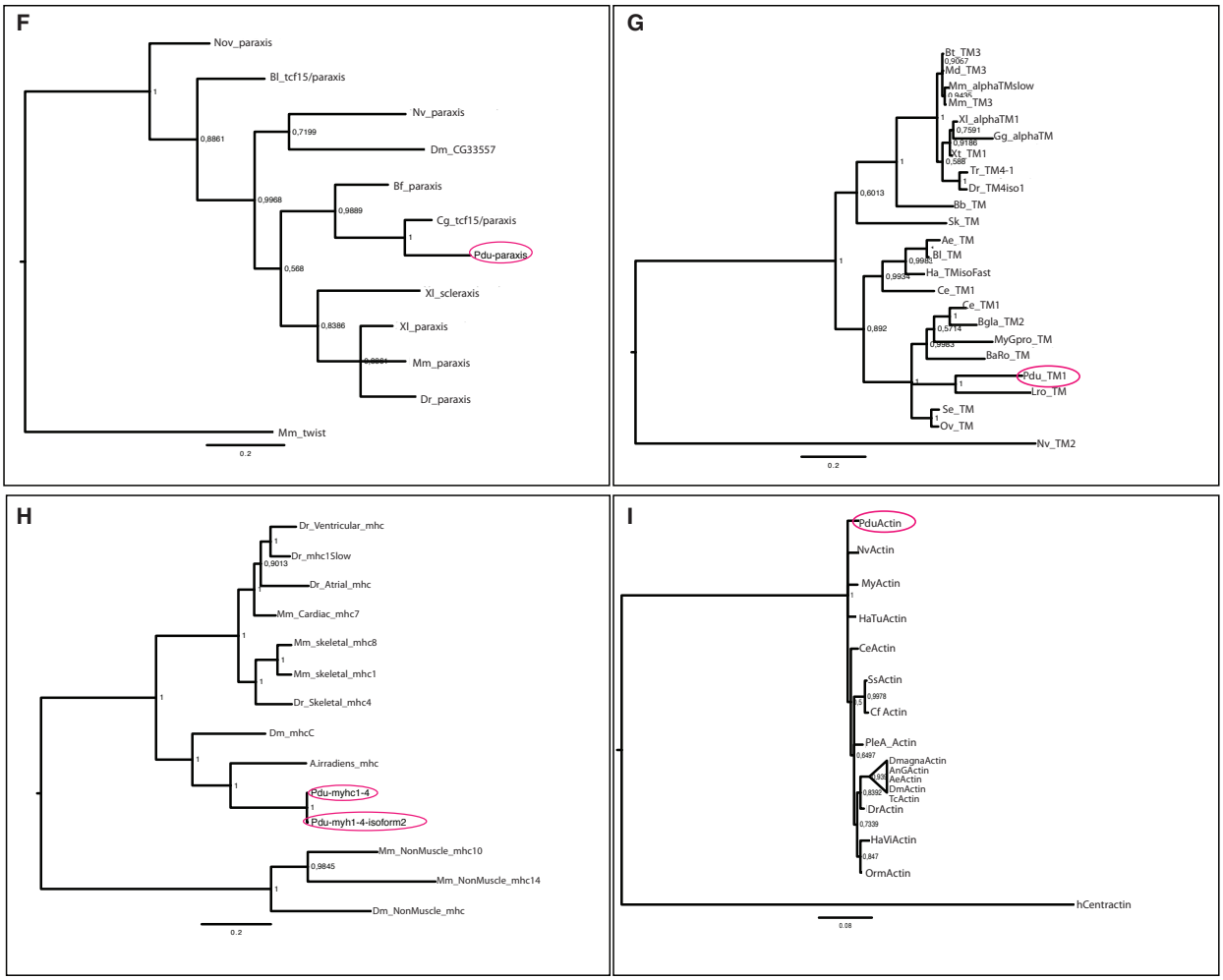

Figure S16. Molecular phylogenies of the genes studied. (**A**) *FoxD*, (**B**) *ColA1* and *ColA2*, (**C**) *Lam-alpha4*, (**D**) *Mox*. (**E**) *Twist* (Twi), (**F**) *Paraxis*, (**G**) *Tropomyosin 1* (TM1), (**H**) *Myosin heavy chain 1-4* (striated myosin heavy chain), (**I**) *Actin. Noggin* orthology has been reported elsewhere (*152*). In all panels, the species names are abbreviated as follows: Pdu (*Platynereis dumerilii*), Dr (*Danio rerio*), Hs (*Homo sapiens*), Xl (*Xenopus laevis*), Bf (*Branchiostoma floridae*), Bb (*Branchiostoma belcheri*), Ce (*Caenorhabditis elegans*), Dpulex (*Daphnia pulex*), Dmagna (*Daphnia magna)*, Dm (*Drosophila melanogaster*), Sk (*Saccoglosus kovalewskii*), Nv (*Nematostella vectensis*), Ct (*Capitella teleta*), HALTU (*Haliotis tuberculata*), EM (*Ephydatia muelleri*), Mm or m (*Mus musculus*), AnG (*Anopheles gambiae*), Nov (*Nasonia vitripennis*), Cg *(Crassostrea gigas),* Bl *(Bombus latreille), Bt (Bos taurus),* MD *(Monodelphis domestica),* TR *(Takifugu rubripes),* Ae *(Aedes aegypti),* Ha *(Homarus americanus),* HaSa *(Haliotis asinina),* Bgla *(Biomphalaria glabrata),* MyGpro *(Mytilus galloprovincialis), BaRo (Balanus rostratus),* LRu *(Lumbricus rubellus),* Se *(Sepia esculenta),* Ov *(Octopus vulgaris),* My *(Mizuhopecten*

yessoensis), HaTu *(Haliotis tuberculata),* Ss *(Sus scrofa),* Cf *(Canis familiaris),* PleA *(Plectus acuminatus),* AnG *(Anopheles gambiae),* HaVi *(Haliotis virescens),* Orm *(Ornithodoros moubata), A.irradiens (Argopectenn irradiens), Subdo (Suberites domuncula).* A: amino acid alignment performed with Muscle and phylogenetic analysis with PhyML (bootstrap values are on the nodes). B-D: amino acid alignment performed with ClustalX and phylogenetic analysis with PhyML (bootstrap values are on the nodes). E-I: amino acid alignment performed with ClustalX and phylogenetic analysis with MrBayes (posterior probabilities are on the nodes).

References and Notes

1. E. M. De Robertis, Y. Sasai, A common plan for dorsoventral patterning in Bilateria. *Nature* **380**, 37–40 (1996). Medline doi:10.1038/380037a0

2. D. L. Stemple, Structure and function of the notochord: An essential organ for chordate development. *Development* **132**, 2503–2512 (2005). Medline doi:10.1242/dev.01812

3. N. Satoh, K. Tagawa, H. Takahashi, How was the notochord born? *Evol. Dev.* **14**, 56–75 (2012). Medline

4. A. S. Denes, G. Jékely, P. R. Steinmetz, F. Raible, H. Snyman, B. Prud'homme, D. E. Ferrier, G. Balavoine, D. Arendt, Molecular architecture of annelid nerve cord supports common origin of nervous system centralization in bilateria. *Cell* **129**, 277–288 (2007). Medline doi:10.1016/j.cell.2007.02.040

5. D. Arendt, K. Nübler-Jung, Dorsal or ventral: Similarities in fate maps and gastrulation patterns in annelids, arthropods and chordates. *Mech. Dev.* **61**, 7–21 (1997). Medline doi:10.1016/S0925-4773(96)00620-X

6. R. Tomer, K. Khairy, F. Amat, P. J. Keller, Quantitative high-speed imaging of entire developing embryos with simultaneous multiview light-sheet microscopy. *Nat. Methods* **9**, 755–763 (2012). Medline doi:10.1038/nmeth.2062

7. J. B. Wallingford, S. E. Fraser, R. M. Harland, Convergent extension: The molecular control of polarized cell movement during embryonic development. *Dev. Cell* **2**, 695–706 (2002). Medline doi:10.1016/S1534-5807(02)00197-1

8. O. Simakov, F. Marletaz, S. J. Cho, E. Edsinger-Gonzales, P. Havlak, U. Hellsten, D. H. Kuo, T. Larsson, J. Lv, D. Arendt, R. Savage, K. Osoegawa, P. de Jong, J. Grimwood, J. A. Chapman, H. Shapiro, A. Aerts, R. P. Otillar, A. Y. Terry, J. L. Boore, I. V. Grigoriev, D. R. Lindberg, E. C. Seaver, D. A. Weisblat, N. H. Putnam, D. S. Rokhsar, Insights into bilaterian evolution from three spiralian genomes. *Nature* **493**, 526–531 (2013). Medline doi:10.1038/nature11696

9. D. Arendt, U. Technau, J. Wittbrodt, Evolution of the bilaterian larval foregut. *Nature* **409**, 81–85 (2001). Medline doi:10.1038/35051075

10. M. Catala, M. A. Teillet, E. M. De Robertis, M. L. Le Douarin, A spinal cord fate map in the avian embryo: While regressing, Hensen's node lays down the notochord and floor plate thus joining the spinal cord lateral walls. *Development* **122**, 2599–2610 (1996). Medline

11. R. Burgess, P. Cserjesi, K. L. Ligon, E. N. Olson, Paraxis: A basic helix-loop-helix protein expressed in paraxial mesoderm and developing somites. *Dev. Biol.* **168**, 296–306 (1995). Medline doi:10.1006/dbio.1995.1081

12. W. E. Reintsch, A. Habring-Mueller, R. W. Wang, A. Schohl, F. Fagotto, beta-Catenin controls cell sorting at the notochord-somite boundary independently of cadherin-mediated adhesion. *J. Cell Biol.* **170**, 675–686 (2005). Medline doi:10.1083/jcb.200503009

13. A. H. Fischer, T. Henrich, D. Arendt, The normal development of *Platynereis dumerilii* (Nereididae, Annelida). *Front. Zool.* **7**, 31 (2010). Medline doi:10.1186/1742-9994-7-31

14. J. E. Webb, The role of the notochard in forward and reverse swimming and burrowing in the amphioxus *Branchiostoma lanceolatum*. *J. Zool.* **170**, 325–338 (1973). doi:10.1111/j.1469-7998.1973.tb01381.x

15. M. M. Suzuki, N. Satoh, Genes expressed in the amphioxus notochord revealed by EST analysis. *Dev. Biol.* **224**, 168–177 (2000). Medline doi:10.1006/dbio.2000.9796

16. D. G. Baskin, Fine structure, functional organization and supportive role of neuroglia in Nereis. *Tissue Cell* **3**, 579–587 (1971). Medline doi:10.1016/S0040-8166(71)80005-8

17. P. D. Currie, P. W. Ingham, Induction of a specific muscle cell type by a hedgehog-like protein in zebrafish. *Nature* **382**, 452–455 (1996). Medline doi:10.1038/382452a0

18. S. D. Hill, B. C. Boyer, Phalloidin labeling of developing muscle in embryos of the polychaete *Capitella* sp. I. *Biol. Bull.* **201**, 257–258 (2001). Medline doi:10.2307/1543353

19. A. Filippova, G. Purschke, A. B. Tzetlin, M. C. M. Müller, Reconstruction of the musculature of *Magelona* cf. *mirabilis* (Magelonidae) and *Prionospio cirrifera* (Spionidae) (Polychaeta, Annelida) by phalloidin labeling and cLSM. *Zoomorphology* **124**, 1–8 (2005). doi:10.1007/s00435-004-0106-7

20. K. K. Dill, K. Thamm, E. C. Seaver, Characterization of twist and snail gene expression during mesoderm and nervous system development in the polychaete annelid *Capitella* sp. I. *Dev. Genes Evol.* **217**, 435–447 (2007). Medline doi:10.1007/s00427-007-0153-4

21. E. C. Seaver, L. M. Kaneshige, Expression of ‘segmentation’ genes during larval and juvenile development in the polychaetes *Capitella* sp. I and H. elegans. *Dev. Biol.* **289**, 179–194 (2006). Medline doi:10.1016/j.ydbio.2005.10.025

22. A. Weigert, C. Helm, M. Meyer, B. Nickel, D. Arendt, B. Hausdorf, S. R. Santos, K. M. Halanych, G. Purschke, C. Bleidorn, T. H. Struck, Illuminating the base of the annelid tree using transcriptomics. *Mol. Biol. Evol.* **31**, 1391–1401 (2014). Medline doi:10.1093/molbev/msu080

23. M. Scherholz, E. Redl, T. Wollesen, C. Todt, A. Wanninger, Aplacophoran mollusks evolved from ancestors with polyplacophoran-like features. *Curr. Biol.* **23**, 2130–2134 (2013). Medline doi:10.1016/j.cub.2013.08.056

24. A. Altenburger, A. Wanninger, Comparative larval myogenesis and adult myoanatomy of the rhynchonelliform (articulate) brachiopods *Argyrotheca cordata*, *A. cistellula*, and *Terebratalia transversa*. *Front. Zool.* **6**, 3 (2009). Medline doi:10.1186/1742-9994-6-3

25. F. Marlétaz, E. Martin, Y. Perez, D. Papillon, X. Caubit, C. J. Lowe, B. Freeman, L. Fasano, C. Dossat, P. Wincker, J. Weissenbach, Y. Le Parco, Chaetognath phylogenomics: A protostome with deuterostome-like development. *Curr. Biol.* **16**, R577–R578 (2006). Medline doi:10.1016/j.cub.2006.07.016

26. F. Marlétaz, A. Gilles, X. Caubit, Y. Perez, C. Dossat, S. Samain, G. Gyapay, P. Wincker, Y. Le Parco, Chaetognath transcriptome reveals ancestral and unique features among bilaterians. *Genome Biol.* **9**, R94 (2008). Medline doi:10.1186/gb-2008-9-6-r94

27. K. J. Peterson, R. A. Cameron, K. Tagawa, N. Satoh, E. H. Davidson, A comparative molecular approach to mesodermal patterning in basal deuterostomes: The expression pattern of Brachyury in the enteropneust hemichordate *Ptychodera flava*. *Development* **126**, 85–95 (1999). Medline

28. J. Gerhart, C. Lowe, M. Kirschner, Hemichordates and the origin of chordates. *Curr. Opin. Genet. Dev.* **15**, 461–467 (2005). Medline doi:10.1016/j.gde.2005.06.004

29. J. Gerhart, The deuterostome ancestor. *J. Cell. Physiol.* **209**, 677–685 (2006). Medline doi:10.1002/jcp.20803

30. N. Miyamoto, H. Wada, Hemichordate neurulation and the origin of the neural tube. *Nat. Commun.* **4**, 2713 (2013). Medline doi:10.1038/ncomms3713

31. J. A. Belo, L. Leyns, G. Yamada, E. M. De Robertis, The prechordal midline of the chondrocranium is defective in Goosecoid-1 mouse mutants. *Mech. Dev.* **72**, 15–25 (1998). Medline doi:10.1016/S0925-4773(97)00204-9

32. E. M. Pera, M. Kessel, Patterning of the chick forebrain anlage by the prechordal plate. *Development* **124**, 4153–4162 (1997). Medline

33. A. W. L. Leung, S. Y. Y. Wong, D. Chan, P. P. L. Tam, K. S. E. Cheah, Loss of procollagen IIA from the anterior mesendoderm disrupts the development of mouse embryonic forebrain. *Dev. Dyn.* **239**, 2319–2329 (2010). Medline doi:10.1002/dvdy.22366

34. K. Nübler-Jung, D. Arendt, Dorsoventral axis inversion: Enteropneust anatomy links invertebrates to chordates turned upside down. *J. Zool. Syst. Evol. Res.* **37**, 93–100 (1999). doi:10.1046/j.1439-0469.1999.372106.x

35. D. Arendt, K. Nübler-Jung, Inversion of dorsoventral axis? *Nature* **371**, 26 (1994). Medline doi:10.1038/371026a0

36. W. S. Talbot, B. Trevarrow, M. E. Halpern, A. E. Melby, G. Farr, J. H. Postlethwait, T. Jowett, C. B. Kimmel, D. Kimelman, A homeobox gene essential for zebrafish notochord development. *Nature* **378**, 150–157 (1995). Medline doi:10.1038/378150a0

37. M. Stefanini, C. De Martino, L. Zamboni, Fixation of ejaculated spermatozoa for electron microscopy. *Nature* **216**, 173–174 (1967). Medline doi:10.1038/216173a0

38. P. D. McCrea, W. M. Brieher, B. M. Gumbiner, Induction of a secondary body axis in *Xenopus* by antibodies to beta-catenin. *J. Cell Biol.* **123**, 477–484 (1993). Medline doi:10.1083/jcb.123.2.477

39. F. Christodoulou, F. Raible, R. Tomer, O. Simakov, K. Trachana, S. Klaus, H. Snyman, G. J. Hannon, P. Bork, D. Arendt, Ancient animal microRNAs and the evolution of tissue identity. *Nature* **463**, 1084–1088 (2010). Medline doi:10.1038/nature08744

40. H. Marlow *et al.*, *BMC Evol. Biol.* (2013).

41. N. Dray, K. Tessmar-Raible, M. Le Gouar, L. Vibert, F. Christodoulou, K. Schipany, A. Guillou, J. Zantke, H. Snyman, J. Béhague, M. Vervoort, D. Arendt, G. Balavoine, Hedgehog signaling regulates segment formation in the annelid *Platynereis*. *Science* **329**, 339–342 (2010). Medline doi:10.1126/science.1188913

42. K. Tessmar-Raible, P. R. H. Steinmetz, H. Snyman, M. Hassel, D. Arendt, Fluorescent two-color whole mount in situ hybridization in *Platynereis dumerilii* (Polychaeta, Annelida), an emerging marine molecular model for evolution and development. *Biotechniques* **39**, 460–464, 462, 464 (2005). Medline doi:10.2144/000112023

43. K. Sakamoto, L. J. Goodyear, Invited review: Intracellular signaling in contracting skeletal muscle. *J. Appl. Physiol.* **93**, 369–383 (2002). Medline

44. S. Q. Schneider, B. Bowerman, beta-Catenin asymmetries after all animal/vegetal-oriented cell divisions in *Platynereis dumerilii* embryos mediate binary cell-fate specification. *Dev. Cell* **13**, 73–86 (2007). Medline doi:10.1016/j.devcel.2007.05.002

45. R. Keller, L. Davidson, A. Edlund, T. Elul, M. Ezin, D. Shook, P. Skoglund, Mechanisms of convergence and extension by cell intercalation. *Philos. Trans. R. Soc. London Ser. B* **355**, 897–922 (2000). Medline doi:10.1098/rstb.2000.0626

46. R. E. Keller, M. Danilchik, R. Gimlich, J. Shih, The function and mechanism of convergent extension during gastrulation of *Xenopus laevis*. *J. Embryol. Exp. Morphol.* **89** (suppl.), 185–209 (1985). Medline

47. J. Shih, R. Keller, Cell motility driving mediolateral intercalation in explants of *Xenopus laevis*. *Development* **116**, 901–914 (1992). Medline

48. P. Wilson, R. Keller, Cell rearrangement during gastrulation of *Xenopus*: Direct observation of cultured explants. *Development* **112**, 289–300 (1991). Medline

49. R. M. Warga, C. B. Kimmel, Cell movements during epiboly and gastrulation in zebrafish. *Development* **108**, 569–580 (1990). Medline

50. N. S. Glickman, C. B. Kimmel, M. A. Jones, R. J. Adams, Shaping the zebrafish notochord. *Development* **130**, 873–887 (2003). Medline doi:10.1242/dev.00314

51. D. Jiang, W. C. Smith, Ascidian notochord morphogenesis. *Dev. Dyn.* **236**, 1748–1757 (2007). Medline doi:10.1002/dvdy.21184

52. D. M. Miyamoto, R. J. Crowther, Formation of the notochord in living ascidian embryos. *J. Embryol. Exp. Morphol.* **86**, 1–17 (1985). Medline

53. E. G. Conklin, The embryology of amphioxus. *J. Morphol.* **54**, 69–151 (1932). doi:10.1002/jmor.1050540103

54. P. W. Holland, B. Koschorz, L. Z. Holland, B. G. Herrmann, Conservation of Brachyury (T) genes in amphioxus and vertebrates: Developmental and evolutionary implications. *Development* **121**, 4283–4291 (1995). Medline

55. K. Terazawa, N. Satoh, Formation of the chordamesoderm in the amphioxus embryo: Analysis with Brachyury and fork head/HNF-3 genes. *Dev. Genes Evol.* **207**, 1–11 (1997). Medline doi:10.1007/s004270050086

56. S. Schulte-Merker, F. J. van Eeden, M. E. Halpern, C. B. Kimmel, C. Nüsslein-Volhard, no tail (ntl) is the zebrafish homologue of the mouse T (Brachyury) gene. *Development* **120**, 1009–1015 (1994). Medline

57. J. C. Smith, B. M. J. Price, J. B. A. Green, D. Weigel, B. G. Herrmann, Expression of a *Xenopus* homolog of Brachyury (T) is an immediate-early response to mesoderm induction. *Cell* **67**, 79–87 (1991). Medline doi:10.1016/0092-8674(91)90573-H

58. F. L. Conlon, J. C. Smith, Interference with brachyury function inhibits convergent extension, causes apoptosis, and reveals separate requirements in the FGF and activin signalling pathways. *Dev. Biol.* **213**, 85–100 (1999). Medline doi:10.1006/dbio.1999.9330

59. A. Kispert, H. Ortner, J. Cooke, B. G. Herrmann, The chick Brachyury gene: Developmental expression pattern and response to axial induction by localized activin. *Dev. Biol.* **168**, 406–415 (1995). Medline doi:10.1006/dbio.1995.1090

60. D. G. Wilkinson, S. Bhatt, B. G. Herrmann, Expression pattern of the mouse T gene and its role in mesoderm formation. *Nature* **343**, 657–659 (1990). Medline doi:10.1038/343657a0

61. S. M. Shimeld, Characterisation of amphioxus HNF-3 genes: Conserved expression in the notochord and floor plate. *Dev. Biol.* **183**, 74–85 (1997). Medline doi:10.1006/dbio.1996.8481

62. J. Odenthal, C. Nüsslein-Volhard, fork head domain genes in zebrafish. *Dev. Genes Evol.* **208**, 245–258 (1998). Medline doi:10.1007/s004270050179

63. M.-L. Dirksen, M. Jamrich, Differential expression of fork head genes during early *Xenopus* and zebrafish development. *Dev. Genet.* **17**, 107–116 (1995). Medline doi:10.1002/dvg.1020170203

64. G. W. Bell, T. A. Yatskievych, P. B. Antin, GEISHA, a whole-mount in situ hybridization gene expression screen in chicken embryos. *Dev. Dyn.* **229**, 677–687 (2004). Medline doi:10.1002/dvdy.10503

65. Q. Ding, J. Motoyama, S. Gasca, R. Mo, H. Sasaki, J. Rossant, C. C. Hui, Diminished Sonic hedgehog signaling and lack of floor plate differentiation in Gli2 mutant mice. *Development* **125**, 2533–2543 (1998). Medline

66. S.-L. Ang, J. Rossant, HNF-3 beta is essential for node and notochord formation in mouse development. *Cell* **78**, 561–574 (1994). Medline doi:10.1016/0092-8674(94)90522-3

67. K. Yasui, S. C. Zhang, M. Uemura, S. Aizawa, T. Ueki, Expression of a twist-related gene, Bbtwist, during the development of a lancelet species and its relation to cephalochordate anterior structures. *Dev. Biol.* **195**, 49–59 (1998). Medline doi:10.1006/dbio.1997.8834

68. I. Germanguz, D. Lev, T. Waisman, C.-H. Kim, I. Gitelman, Four twist genes in zebrafish, four expression patterns. *Dev. Dyn.* **236**, 2615–2626 (2007). Medline doi:10.1002/dvdy.21267

69. N. D. Hopwood, A. Pluck, J. B. Gurdon, A *Xenopus* mRNA related to *Drosophila* twist is expressed in response to induction in the mesoderm and the neural crest. *Cell* **59**, 893–903 (1989). Medline doi:10.1016/0092-8674(89)90612-0

70. C. Zhang, M. W. Klymkowsky, Unexpected functional redundancy between Twist and Slug (Snail2) and their feedback regulation of NF-kappaB via Nodal and Cerberus. *Dev. Biol.* **331**, 340–349 (2009). Medline doi:10.1016/j.ydbio.2009.04.016

71. M. Scaal, E.-M. Füchtbauer, B. Brand-Saberi, cDermo-1 expression indicates a role in avian skin development. *Anat. Embryol.* **203**, 1–7 (2001). Medline doi:10.1007/PL00008244

72. L. Li, P. Cserjesi, E. N. Olson, Dermo-1: A novel twist-related bHLH protein expressed in the developing dermis. *Dev. Biol.* **172**, 280–292 (1995). Medline doi:10.1006/dbio.1995.0023

73. J.-K. Yu, N. D. Holland, L. Z. Holland, An amphioxus winged helix/forkhead gene, AmphiFoxD: Insights into vertebrate neural crest evolution. *Dev. Dyn.* **225**, 289–297 (2002). Medline doi:10.1002/dvdy.10173

74. S. Dutta, I. B. Dawid, Kctd15 inhibits neural crest formation by attenuating Wnt/beta-catenin signaling output. *Development* **137**, 3013–3018 (2010). Medline doi:10.1242/dev.047548

75. M. Sölter, M. Köster, T. Hollemann, A. Brey, T. Pieler, W. Knöchel, Characterization of a subfamily of related winged helix genes, XFD-12/12′/12″ (XFLIP), during *Xenopus* embryogenesis. *Mech. Dev.* **89**, 161–165 (1999). Medline doi:10.1016/S0925-4773(99)00195-1

76. A. B. Steiner, M. J. Engleka, Q. Lu, E. C. Piwarzyk, S. Yaklichkin, J. L. Lefebvre, J. W. Walters, L. Pineda-Salgado, P. A. Labosky, D. S. Kessler, FoxD3 regulation of Nodal in the Spemann organizer is essential for *Xenopus* dorsal mesoderm development. *Development* **133**, 4827–4838 (2006). Medline doi:10.1242/dev.02663

77. J. Khudyakov, M. Bronner-Fraser, Comprehensive spatiotemporal analysis of early chick neural crest network genes. *Dev. Dyn.* **238**, 716–723 (2009). Medline doi:10.1002/dvdy.21881

78. H. Sasaki, B. L. Hogan, Differential expression of multiple fork head related genes during gastrulation and axial pattern formation in the mouse embryo. *Development* **118**, 47–59 (1993). Medline

79. O. J. Tamplin, B. J. Cox, J. Rossant, Integrated microarray and ChIP analysis identifies multiple Foxa2 dependent target genes in the notochord. *Dev. Biol.* **360**, 415–425 (2011). Medline doi:10.1016/j.ydbio.2011.10.002

80. D. Meulemans, M. Bronner-Fraser, Insights from amphioxus into the evolution of vertebrate cartilage. *PLOS ONE* **2**, e787 (2007). Medline doi:10.1371/journal.pone.0000787

81. P. Smits, V. Lefebvre, Sox5 and Sox6 are required for notochord extracellular matrix sheath formation, notochord cell survival and development of the nucleus pulposus of intervertebral discs. *Development* **130**, 1135–1148 (2003). Medline doi:10.1242/dev.00331

82. M. Li, C. Zhao, Y. Wang, Z. Zhao, A. Meng, Zebrafish sox9b is an early neural crest marker. *Dev. Genes Evol.* **212**, 203–206 (2002). Medline doi:10.1007/s00427-002-0235-2

83. Y.-H. Lee, J.-P. Saint-Jeannet, Sox9, a novel pancreatic marker in *Xenopus*. *Int. J. Dev. Biol.* **47**, 459–462 (2003). Medline

84. S. J. McKeown, V. M. Lee, M. Bronner-Fraser, D. F. Newgreen, P. G. Farlie, Sox10 overexpression induces neural crest-like cells from all dorsoventral levels of the neural tube but inhibits differentiation. *Dev. Dyn.* **233**, 430–444 (2005). Medline doi:10.1002/dvdy.20341

85. L. J. Ng, S. Wheatley, G. E. Muscat, J. Conway-Campbell, J. Bowles, E. Wright, D. M. Bell, P. P. Tam, K. S. Cheah, P. Koopman, SOX9 binds DNA, activates transcription, and coexpresses with type II collagen during chondrogenesis in the mouse. *Dev. Biol.* **183**, 108–121 (1997). Medline doi:10.1006/dbio.1996.8487

86. C. Thisse, B. Thisse, "High throughput expression analysis of ZF-Models Consortium clones," in ZFIN Direct Data Submission (2013); http://zfin.org.

87. J. H. Chen, W. Wu, H. S. Li, T. Fagaly, L. Zhou, J. Y. Wu, Y. Rao, Embryonic expression and extracellular secretion of *Xenopus* slit. *Neuroscience* **96**, 231–236 (2000). Medline doi:10.1016/S0306-4522(99)00408-X

88. G. Holmes, L. Niswander, Expression of slit-2 and slit-3 during chick development. *Dev. Dyn.* **222**, 301–307 (2001). Medline doi:10.1002/dvdy.1182

89. G. P. Holmes, K. Negus, L. Burridge, S. Raman, E. Algar, T. Yamada, M. H. Little, Distinct but overlapping expression patterns of two vertebrate slit homologs implies functional roles in CNS development and organogenesis. *Mech. Dev.* **79**, 57–72 (1998). Medline doi:10.1016/S0925-4773(98)00174-9

90. B. J. Dickson, G. F. Gilestro, Regulation of commissural axon pathfinding by slit and its Robo receptors. *Annu. Rev. Cell Dev. Biol.* **22**, 651–675 (2006). Medline doi:10.1146/annurev.cellbio.21.090704.151234

91. S. Shimeld, An amphioxus netrin gene is expressed in midline structures during embryonic and larval development. *Dev. Genes Evol.* **210**, 337–344 (2000). Medline doi:10.1007/s004270000073

92. K. W. Park, L. D. Urness, M. M. Senchuk, C. J. Colvin, J. D. Wythe, C.-B. Chien, D. Y. Li, Identification of new netrin family members in zebrafish: Developmental expression of netrin 2 and netrin 4. *Dev. Dyn.* **234**, 726–731 (2005). Medline doi:10.1002/dvdy.20474

93. T. E. Kennedy, T. Serafini, J. R. de la Torre, M. Tessier-Lavigne, Netrins are diffusible chemotropic factors for commissural axons in the embryonic spinal cord. *Cell* **78**, 425–435 (1994). Medline doi:10.1016/0092-8674(94)90421-9

94. S. M. Shimeld, The evolution of the hedgehog gene family in chordates: Insights from amphioxus hedgehog. *Dev. Genes Evol.* **209**, 40–47 (1999). Medline doi:10.1007/s004270050225

95. S. Krauss, J. P. Concordet, P. W. Ingham, A functionally conserved homolog of the *Drosophila* segment polarity gene hh is expressed in tissues with polarizing activity in zebrafish embryos. *Cell* **75**, 1431–1444 (1993). Medline doi:10.1016/0092-8674(93)90628-4

96. S. C. Ekker, L. L. McGrew, C. J. Lai, J. J. Lee, D. P. von Kessler, R. T. Moon, P. A. Beachy, Distinct expression and shared activities of members of the hedgehog gene family of *Xenopus laevis*. *Development* **121**, 2337–2347 (1995). Medline

97. E. Martí, R. Takada, D. A. Bumcrot, H. Sasaki, A. P. McMahon, Distribution of Sonic hedgehog peptides in the developing chick and mouse embryo. *Development* **121**, 2537–2547 (1995). Medline

98. Y. Echelard, D. J. Epstein, B. St-Jacques, L. Shen, J. Mohler, J. A. McMahon, A. P. McMahon, Sonic hedgehog, a member of a family of putative signaling molecules, is implicated in the regulation of CNS polarity. *Cell* **75**, 1417–1430 (1993). Medline doi:10.1016/0092-8674(93)90627-3

99. Y. Tanabe, H. Roelink, T. M. Jessell, Induction of motor neurons by Sonic hedgehog is independent of floor plate differentiation. *Curr. Biol.* **5**, 651–658 (1995). Medline doi:10.1016/S0960-9822(95)00130-8

100. F. Charron, E. Stein, J. Jeong, A. P. McMahon, M. Tessier-Lavigne, The morphogen sonic hedgehog is an axonal chemoattractant that collaborates with netrin-1 in midline axon guidance. *Cell* **113**, 11–23 (2003). Medline doi:10.1016/S0092-8674(03)00199-5

101. M. Fürthauer, B. Thisse, C. Thisse, Three different noggin genes antagonize the activity of bone morphogenetic proteins in the zebrafish embryo. *Dev. Biol.* **214**, 181–196 (1999). Medline doi:10.1006/dbio.1999.9401

102. W. C. Smith, R. M. Harland, Expression cloning of noggin, a new dorsalizing factor localized to the Spemann organizer in *Xenopus* embryos. *Cell* **70**, 829–840 (1992). Medline doi:10.1016/0092-8674(92)90316-5

103. J. A. McMahon, S. Takada, L. B. Zimmerman, C. M. Fan, R. M. Harland, A. P. McMahon, Noggin-mediated antagonism of BMP signaling is required for growth and patterning of the neural tube and somite. *Genes Dev.* **12**, 1438–1452 (1998). Medline doi:10.1101/gad.12.10.1438

104. Q. Ding, W. Xia, J. C. Liu, J. Y. Yang, D. F. Lee, J. Xia, G. Bartholomeusz, Y. Li, Y. Pan, Z. Li, R. C. Bargou, J. Qin, C. C. Lai, F. J. Tsai, C. H. Tsai, M. C. Hung, Erk associates with and primes GSK-3beta for its inactivation resulting in upregulation of beta-catenin. *Mol. Cell* **19**, 159–170 (2005). Medline doi:10.1016/j.molcel.2005.06.009

105. M. W. Su, H. R. Suzuki, J. J. Bieker, M. Solursh, F. Ramirez, Expression of two nonallelic type II procollagen genes during Xenopus laevis embryogenesis is characterized by stage-specific production of alternatively spliced transcripts. *J. Cell Biol.* **115**, 565–575 (1991). Medline doi:10.1083/jcb.115.2.565

106. A. J. Bendall, G. Hu, G. Levi, C. Abate-Shen, Dlx5 regulates chondrocyte differentiation at multiple stages. *Int. J. Dev. Biol.* **47**, 335–344 (2003). Medline

107. R. A. Kosher, M. Solursh, Widespread distribution of type II collagen during embryonic chick development. *Dev. Biol.* **131**, 558–566 (1989). Medline doi:10.1016/S0012-1606(89)80026-0

108. A. Wood, D. E. Ashhurst, A. Corbett, P. Thorogood, The transient expression of type II collagen at tissue interfaces during mammalian craniofacial development. *Development* **111**, 955–968 (1991). Medline

109. A. Aszódi, D. Chan, E. Hunziker, J. F. Bateman, R. Fässler, Collagen II is essential for the removal of the notochord and the formation of intervertebral discs. *J. Cell Biol.* **143**, 1399–1412 (1998). Medline doi:10.1083/jcb.143.5.1399

110. D. Leiss, U. Hinz, A. Gasch, R. Mertz, R. Renkawitz-Pohl, Beta 3 tubulin expression characterizes the differentiating mesodermal germ layer during *Drosophila* embryogenesis. *Development* **104**, 525–531 (1988). Medline

111. E. S. Goodrich, *Studies on the Structure and Development of Vertebrates* (Macmillan, City, Country, ed. 1, 1930).

112. P.-P. Grassé, *Traite de Zoologie: Anatomie, Systematique, Biologie Tome XI* (Masson, City, France, 1948).

113. T. Cedhagen, H. G. Hansson, Biology and distribution of hemichordates (Enteropneusta) with emphasis on Harrimaniidae and description of *Protoglossus bocki* sp. nov. from Scandinavia. *Helgol. Mar. Res.* **67**, 251–265 (2013). doi:10.1007/s10152-012-0320-5

114. T. Stach, A. Gruhl, S. Kaul-Strehlow, The central and peripheral nervous system of *Cephalodiscus gracilis* (Pterobranchia, Deuterostomia). *Zoomorphology* **131**, 11–24 (2012). doi:10.1007/s00435-011-0144-x

115. V. Dyachuk, N. Odintsova, Larval myogenesis in Echinodermata: Conserved features and morphological diversity between class-specific larval forms of

Echinoidae, Asteroidea, and Holothuroidea. *Evol. Dev.* **15**, 5–17 (2013). Medline doi:10.1111/ede.12010

116. G. L. Shinn, *Am. Zool.* **34**, 523–532 (1994).

117. G. L. Shinn, M. E. Roberts, Ultrastructure of hatchling chaetognaths (*Ferosagitta hispida*): Epithelial arrangement of the mesoderm and its phylogenetic implications. *J. Morphol.* **219**, 143–163 (1994). doi:10.1002/jmor.1052190204

118. R. C. Neves, X. Bailly, F. Leasi, H. Reichert, M. V. Sørensen, R. M. Kristensen, A complete three-dimensional reconstruction of the myoanatomy of Loricifera: Comparative morphology of an adult and a Higgins larva stage. *Front. Zool.* **10**, 19 (2013). Medline doi:10.1186/1742-9994-10-19

119. M. C. M. Müller, A. Schmidt-Rhaesa, Reconstruction of the muscle system in *Antygomonas* sp. (Kinorhyncha, Cyclorhagida) by means of phalloidin labeling and cLSM. *J. Morphol.* **256**, 103–110 (2003). Medline doi:10.1002/jmor.10058

120. A. Schmidt-Rhaesa, *Nematomorpha*, *Priapulida*, *Kinorhyncha*, *Loricifera* (Walter de Gruyter, City, Country, 2012).

121. R. C. Brusca, G. J. Brusca, *Invertebrates - Second Edition* (Sinauer, City, Country, ed. 2, 2003).

122. J. Zantke, C. Wolff, G. Scholtz, Three-dimensional reconstruction of the central nervous system of *Macrobiotus hufelandi* (Eutardigrada, Parachela): Implications for the phylogenetic position of Tardigrada. *Zoomorphology* **127**, 21–36 (2008). doi:10.1007/s00435-007-0045-1

123. G. Hoyle, M. Williams, The musculature of peripatus and its innervation. *Philos. Trans. R. Soc. London Ser. B* **288**, 481–510 (1980). doi:10.1098/rstb.1980.0024

124. C. Chiang, N. H. Patel, K. E. Young, P. A. Beachy, The novel homeodomain gene buttonless specifies differentiation and axonal guidance functions of *Drosophila* dorsal median cells. *Development* **120**, 3581–3593 (1994). Medline

125. S. Santagata, Larval development of *Phoronis pallida* (Phoronida): Implications for morphological convergence and divergence among larval body plans. *J. Morphol.* **259**, 347–358 (2004). Medline doi:10.1002/jmor.10205

126. P. Funch, The chordoid larva of *Symbion pandora* (Cycliophora) is a modified trochophore. *J. Morphol.* **230**, 231–263 (1996). doi:10.1002/(SICI)1097-4687(199612)230:3<231::AID-JMOR1>3.0.CO;2-H

127. R. C. Neves, R. M. Kristensen, A. Wanninger, Three-dimensional reconstruction of the musculature of various life cycle stages of the cycliophoran *Symbion americanus*. *J. Morphol.* **270**, 257–270 (2009). Medline doi:10.1002/jmor.10681

128. A. Wanninger, Immunocytochemistry of the nervous system and the musculature of the chordoid larva of *Symbion pandora* (Cycliophora). *J. Morphol.* **265**, 237–243 (2005). Medline doi:10.1002/jmor.10354

129. N. Santo, D. Fontaneto, U. Fascio, G. Melone, M. Caprioli, in *Rotifera X: Rotifer Research: Trends, New Tools, and Recent Advances*, A. Herzig, R. D. Gulati, C.

D. Jersabek, L. May, Eds., vol. 181 of *Developments in Hydrobiology* (Springer, Dordrecht, Netherlands, 2005), pp. 223–229.

130. M. V. Sørensen, Musculature in three species of *Proales* (Monogononta, Rotifera) stained with phalloidin-labeled fluorescent dye. *Zoomorphology* **124**, 47–55 (2005). doi:10.1007/s00435-005-0110-6

131. O. Riemann, P. Martínez Arbizu, A. Kieneke, Organisation of body musculature in *Encentrum mucronatum* Wulfert, 1936, *Dicranophorus forcipatus* (O. F. Müller, 1786) and in the ground pattern of Ploima (Rotifera: Monogononta). *Zool. Anz. J. Comp. Zool.* **247**, 133–145 (2008). doi:10.1016/j.jcz.2007.09.004

132. M. Müller, W. Sterrer, *Zoomorphology* **123**, 169–177 (2004).

133. F. Leasi, M. A. Todaro, The muscular system of *Musellifer delamarei* (Renaud-Mornant, 1968) and other chaetonotidans with implications for the phylogeny and systematization of the Paucitubulatina (Gastrotricha). *Biol. J. Linn. Soc. London* **94**, 379–398 (2008). doi:10.1111/j.1095-8312.2008.00974.x

134. F. Leasi, M. A. Todaro, Meiofaunal cryptic species revealed by confocal microscopy: The case of *Xenotrichula intermedia* (Gastrotricha). *Mar. Biol.* **156**, 1335–1346 (2009). doi:10.1007/s00227-009-1175-4

135. R. Hochberg, M. Klauser Litvaitis, *Hydrobiologia* **452**, 155–161 (2001). doi:10.1023/A:1011940430507

136. S. T. Spindle, thesis, Virginia Commonwealth University, Richmond, VA (2013); https://digarchive.library.vcu.edu/handle/10156/4474.

137. C. Nielsen, G. Haszprunar, B. Ruthensteiner, A. Wanninger, Early development of the aplacophoran mollusc Chaetoderma. *Acta Zool.* **88**, 231–247 (2007). doi:10.1111/j.1463-6395.2007.00270.x

138. L. H. Hyman, *Invertebrates: Mollusca I* (McGraw-Hill, City, Country, 1967).

139. J. Rüchel, M. C. M. Müller, F-actin framework in *Spirorbis* cf. *spirorbis* (Annelida: Serpulidae): Phalloidin staining investigated and reconstructed by cLSM. *Invertebr. Biol.* **126**, 173–182 (2007). doi:10.1111/j.1744-7410.2007.00087.x

140. N. Brinkmann, A. Wanninger, Integrative analysis of polychaete ontogeny: Cell proliferation patterns and myogenesis in trochophore larvae of *Sabellaria alveolata*. *Evol. Dev.* **12**, 5–15 (2010). Medline doi:10.1111/j.1525-142X.2009.00386.x

141. A. Filippova, G. Purschke, A. B. Tzetlin, M. C. M. Müller, *Sci. Mar.* **70**, (2007). 10.3989/scimar.2006.70s3293

142. M. C. M. Müller, K. Worsaae, CLSM analysis of the phalloidin-stained muscle system in *Nerilla antennata*, *Nerillidium* sp. and *Trochonerilla mobilis* (Polychaeta; Nerillidae). *J. Morphol.* **267**, 885–896 (2006). Medline doi:10.1002/jmor.10292

143. A. B. Tzetlin, A. Zhadan, I. Ivanov, M. C. M. Müller, G. Purschke, On the absence of circular muscle elements in the body wall of *Dysponetus pygmaeus*

(Chrysopetalidae, ‘Polychaeta’, Annelida). *Acta Zool.* **83**, 81–85 (2002). doi:10.1046/j.1463-6395.2002.00104.x

144. A. Filippova, G. Purschke, A. B. Tzetlin, M. C. M. Müller, Musculature in polychaetes: Comparison of *Myrianida prolifera* (Syllidae) and *Sphaerodoropsis* sp. (Sphaerodoridae). *Invertebr. Biol.* **129**, 184–198 (2010). doi:10.1111/j.1744-7410.2010.00191.x

145. G. Purschke, M. C. M. Müller, Evolution of body wall musculature. *Integr. Comp. Biol.* **46**, 497–507 (2006). Medline doi:10.1093/icb/icj053

146. A. Kristof, T. Wollesen, A. S. Maiorova, A. Wanninger, Cellular and muscular growth patterns during sipunculan development. *J. Exp. Zool. B Mol. Dev. Evol.* **316B**, 227–240 (2011).doi:10.1002/jez.b.21394 Medline

147. M. J. Boyle, E. C. Seaver, Expression of FoxA and GATA transcription factors correlates with regionalized gut development in two lophotrochozoan marine worms: Chaetopterus (Annelida) and *Themiste lageniformis* (Sipuncula). *EvoDevo* **1**, 2 (2010). Medline doi:10.1186/2041-9139-1-2

148. C. McDougall, W.-C. Chen, S. M. Shimeld, D. E. K. Ferrier, The development of the larval nervous system, musculature and ciliary bands of *Pomatoceros lamarckii* (Annelida): Heterochrony in polychaetes. *Front. Zool.* **3**, 16 (2006). Medline doi:10.1186/1742-9994-3-16

149. C. Nielsen, *Animal Evolution: Interrelationships of the Living Phyla* (Oxford Univ. Press, New York, ed. 3, 2012).

150. C. W. Dunn, A. Hejnol, D. Q. Matus, K. Pang, W. E. Browne, S. A. Smith, E. Seaver, G. W. Rouse, M. Obst, G. D. Edgecombe, M. V. Sørensen, S. H. Haddock, A. Schmidt-Rhaesa, A. Okusu, R. M. Kristensen, W. C. Wheeler, M. Q. Martindale, G. Giribet, Broad phylogenomic sampling improves resolution of the animal tree of life. *Nature* **452**, 745–749 (2008). Medline doi:10.1038/nature06614

151. A. Hejnol, M. Obst, A. Stamatakis, M. Ott, G. W. Rouse, G. D. Edgecombe, P. Martinez, J. Baguñà, X. Bailly, U. Jondelius, M. Wiens, W. E. G. Müller, E. Seaver, W. C. Wheeler, M. Q. Martindale, G. Giribet, C. W. Dunn, Assessing the root of bilaterian animals with scalable phylogenomic methods. *Proc. R. Soc. London Ser. B* **276**, 4261–4270 (2009).doi:10.1098/rspb.2009.0896 Medline

152. H. Marlow, M. A. Tosches, R. Tomer, P. R. Steinmetz, A. Lauri, T. Larsson, D. Arendt, Larval body patterning and apical organs are conserved in animal evolution. *BMC Biol.* **12**, 7 (2014). Medline doi:10.1186/1741-7007-12-7